Emerald: A Stochastic Modelling Approach for Rapid Assessment of Groundwater Dynamics

D.J.J. Walvoort
M.F.P. Bierkens

Report 171

DLO Winand Staring Centre, Wageningen (The Netherlands), 1999

ABSTRACT

Walvoort, D.J.J. and M.F.P. Bierkens, 1999. *Emerald: A Stochastic Modelling Approach for Rapid Assessment of Groundwater Dynamics.* Wageningen (The Netherlands), DLO Winand Staring Centre. Report 171. 82 pp.; 16 Figs; 8 Tables; 24 Refs; 6 Annexes.

A simple one-dimensional stochastic model was developed for quantifying groundwater dynamics and model accuracy. Due to its soil physical backbone, the model is somewhere between pure empirical models on the one hand, and complex physical-mechanistic models on the other. Hence, it is envisaged that it is more effective in scenario studies than pure empirical models, and more easily to operate than complex physical-mechanistic models. A case study showed that the model was capable of predicting various groundwater characteristics.

Keywords: groundwater dynamics, stochastic mechanistic model, groundwater depth, specific groundwater discharge, soil physics, transfer function model

ISSN 0927-4537

This report can be ordered by paying 35,00 Dutch guilders into bank account numer 36 70 54 612 in the name of DLO-Staring Centrum, Wageningen, the Netherlands, with reference to Report 171. This amount is inclusive of VAT and postage.

P.O. Box 125, NL-6700 AC Wageningen (The Netherlands)
Phone: 31 (317) 474200; fax: 31 (317) 424812; e-mail: postkamer@sc.dlo.nl

Project 328-80670 [Rep171/HM/07.99]

Contents

Annexes

List of symbols

Note: Dimensions are given in square brackets, *i.e.* []. The dimensions encountered in this report are (combinations of) length [L], and time [t]. Dimensionless quantities are given by [-].

symbol	description	dimension
d_c	critical depth	[L]
d_{ac}	thickness of the soil layer directly under the root zone that is characterized by a pressure head at the bottom equal to the air-entry potential (about pF 1.3)	[L]
d_r	effective rooting depth	[L]
$\hat{C}$	estimated autocovariance function	see text
D	effective drainage depth	[L]
E_a	actual evapotranspiration	$[Lt^{-1}]$
E_p	potential evapotranspiration	$[Lt^{-1}]$
E_r	Makkink's reference-crop evapotranspiration	$[Lt^{-1}]$
f_b	fraction of bypass flow	[-]
f_c	crop factor	[-]
f_{obj}	objective function	[L]
h, H	groundwater level with respect to drainage base	[L]
Y	observed groundwater level	[L]
h_p	pressure head	[L]
J	reservoir characteristic	[t]
k	hydraulic conductivity	$[Lt^{-1}]$
L	average distance between water courses	[L]
n	Van Genuchten parameter	[-]
n_Y	number of observations	[-]
n_L	number of soil layers in percolation zone	[-]
P	precipitation	$[Lt^{-1}]$
q_c	capillary rise	$[Lt^{-1}]$
q_c^{max}	maximum amount of capillary rise	$[Lt^{-1}]$
q_d, Q_d	specific groundwater discharge	$[Lt^{-1}]$
q_g	groundwater recharge	$[Lt^{-1}]$
q_j	outflow of layer j	$[Lt^{-1}]$
q_v	seepage ($q_v>0$) or infiltration ($q_v<0$)	$[Lt^{-1}]$
q_n, Q_n	net input to the groundwater system	$[Lt^{-1}]$
q_p	percolation	$[Lt^{-1}]$
q_s	discharge per unit length of water course	$[L^2t^{-1}]$
q_x	flux density in horizontal direction	$[Lt^{-1}]$
q_z	flux density in vertical direction	$[Lt^{-1}]$
S	step response	[-]
S_h	step response of h	[-]

List of symbols (continued)

symbol	description	dimension
S_p	step response of the percolation zone	[-]
S_{q_d}	step response of q_d	[-]
S_{max}	soil moisture storage capacity of the root zone	[L]
t	time	[t]
t_k	time step k, or time k (depends on the context)	[t]
Δt	duration of time step t_k	[t]
Δt_Y	time step between succeeding observations	[t]
U	pulse response	[-]
U_h	pulse response of h	[-]
U_p	pulse response of the percolation zone	[-]
U_{p_j}	pulse response for layer j of the percolation zone	[-]
U_{q_d}	pulse response of q_d	[-]
V	actual volume of soil moisture in root zone	[L]
V_{min}	minimum volume of soil moisture in root zone	[L]
V_{max}	maximum volume of soil moisture in root zone	[L]
N	autoregressive process of order 1	see context
x	x-coordinate	[L]
z	vertical space coordinate	[L]
z_c	critical depth minus thickness capillary fringe	[L]
z_i	point of inflection of logistic function	[L]
z_s	ground level with respect to drainage base	[L]
α	Van Genuchten parameter	[-]
α_s	reduction factor	[-]
γ	drainage resistance	[t]
δ	autoregressive parameter of deterministic model	[-]
μ	specific yield	[-]
θ	soil moisture content	[-]
θ_{eff}	effective soil moisture content	[-]
θ_{fc}	soil moisture content at field capacity	[-]
θ_r	Van Genuchten parameter	[-]
θ_s	Van Genuchten parameter	[-]
θ_{wp}	soil moisture content at wilting point	[-]
ε	discrete-time white noise	see context
σ_ε^2	variance of white noise	$[L^2t^{-2}]$
τ	lag	[-]
ϕ	autoregressive parameter	[-]
ω_0	moving average parameter of H	[t]
ω_1	moving average parameter of H	[t]
ω_0'	moving average parameter of Q_d	[-]
ω_0'	moving average parameter of Q_d	[-]

Preface

As part of the DWK Research Program 328 of the Dutch Ministry of Agriculture, Nature Conservation, and Fisheries, the section Land Inventory Methods of the Winand Staring Centre is developing a tool-box for characterising groundwater dynamics on local and regional scales. One of the tools in this box is EMERALD, a stochastic hydrologic model, primarily developed to combine fast outcomes with high accuracy. These properties are also reflected by the title of this report, which is in fact derived from the acronym SMARAGD, *i.e.* EMERALD in Dutch.

EMERALD is named after the green variety of the mineral beryl. Beryl is colourless when pure, but intense green when impurities of the metal chromium are present in its crystal lattice. Emerald does not only owe its brilliant green colour to these impurities, but also its preciousness.

The same is true for the mechanistic hydrologic model presented in this report. It is also enriched by adding impurities to its internal structure. But unlike the gem, these impurities are not present in a physical sense, but merely in the form of statistical noise.

We thank Martin Knotters and Tom Hoogland of SC-DLO for their useful comments on an earlier draft of this report.

Summary

Accurate information on phreatic groundwater dynamics is indispensable for agriculture, land use planning, nature conservation, and water management. In addition to field surveys, hydrological models can be very valuable to obtain this information. Due to our incomplete knowledge of the hydrological processes involved (resulting in invalid model assumptions and uncertain model parameters), and input data afflicted with measurement errors, model predictions are inaccurate. Stochastic models can take these uncertainties explicitly into account.

In this report, a stochastic model is presented, which combines the fastness and simplicity of empirical models and the knowledge on soil physics incorporated in physical-mechanistic models. This model, hereafter referred to as EMERALD, consists of three submodels, *i.e.* a model of the unsaturated zone, a model of the saturated zone, and a noise model. The unsaturated zone is partitioned into two subsystems, *i.e.* a root zone and a percolation zone. The root zone is modelled by means of a nonlinear reservoir. The incoming fluxes are precipitation and capillary rise, the outgoing fluxes are evapotranspiration and percolation. The second subsystem, *i.e.* the percolation zone, is modelled as the convolution of the percolation flux leaving the root zone, and the pulse response of the percolation zone. The pulse response is based on Richards' equation, and as such it has a soil physical background. EMERALD can take multiple subsoil layers, and even preferential flow (bypass flow) into account. The saturated zone is modelled by means of an analytical solution to the one-dimensional transient flow equation.

Uncertainty is modelled by means of an autoregressive noise model. This model can be used to generate external or internal noise. External noise is added directly to the predicted time series. Internal noise on the other hand is considered as additional groundwater recharge, and as such it serves as input to the groundwater model. Realizations generated by an internal noise model, therefore contain noise that is affected by the groundwater system. This approach distinguishes EMERALD from most other stochastic hydrological models.

EMERALD can be used to predict time series of groundwater depths at a specific location, together with the variance of the prediction errors. Furthermore, EMERALD can be used to simulate equiprobable realizations of groundwater time series. These realizations can then be used to derive interesting groundwater characteristics like mean highest and mean lowest water table depths, regime curves and frequency of exceedance graphs. Furthermore, the accuracy of the results is explicitly quantified. EMERALD not only generates time series of groundwater depths, but also of specific groundwater discharge, and several additional quantities like actual evapotranspiration, soil moisture content and groundwater recharge.

In this report, four calibration methods are presented. Three pertain to the noise model, and one to the deterministic component of EMERALD. The performance of these methods is tested by means of a simulation study. The calibration method for

the deterministic component of EMERALD performed very well, even in the presence of high noise levels. Calibration of the internal noise model was more difficult. The calibration method pertaining to the external noise model was not tested, because similar methods were tested elsewhere.

The report is concluded with a case study. In this case study EMERALD is confronted with real-wold data. Observed time series were split into calibration and validation sets. EMERALD yielded unbiased predictions for the calibration sets and slightly biased predictions for the validation sets. The accuracy attained, as expressed by the root mean squared error, varied between 11.0 cm and 13.4 cm. The fraction of residuals outside the area bounded by the 2.5% and 97.5% percentiles was generally somewhat too high.

Validation also showed that EMERALD correctly reproduces univariate and bivariate statistics. In addition, derived measures of groundwater dynamics like the mean highest and mean lowest water-table depths, and the frequency of exceedance graph were also predicted well.

EMERALD is implemented in a computer program. It is driven by a simple script language.

1 Introduction

To support policymaking, accurate information on the spatial and temporal variation of groundwater levels is required. In the Netherlands, this kind of information is usually available in the form of maps of water table classes (*e.g.* Te Riele & Brus, 1996). The concept of water table classes provides a concise way to describe groundwater fluctuation by means of two parameters, *i.e.* the mean highest and mean lowest groundwater level (Van der Sluijs, 1990). However, the information provided by these parameters is often too limited. There is a growing need for more detailed information on groundwater dynamics.

This kind of detail can not be obtained by intensifying field survey campaigns, since the required observation density, both in space and time, will certainly violate budgetary constraints. Therefore, in addition to field surveys, one also has to resort to mathematical models for predicting groundwater characteristics at unvisited points in the space-time domain.

One way to describe the spatio-temporal variation of the phreatic surface is to use a distributed transient groundwater model. These models are mechanistic in nature, and describe flow in the saturated zone. However, the spatial variation of a shallow water table is mostly determined by the properties of the unsaturated zone, and by a dense network of drainage ditches with controlled surface water levels. To describe such groundwater tables with sufficient accuracy (root mean squared prediction error smaller than 20 cm), the distributed groundwater model must be of high resolution, and should include the unsaturated zone and all surface waters. This would require an enormous amount of input that can only be acquired at high costs.

Alternatively, one can use simple one-dimensional models of soil-groundwater interaction that describe the temporal variation of the water table at a single location. Such one dimensional models only require some meteorological inputs and simple borehole descriptions of the topsoil (of which there are many available at the Staring Centre). At each point where a borehole description is available, one-dimensional models can be used to generate long time series of daily water table depths. A spatio-temporal description then follows from interpolating between these locations.

Knotters & Van Walsum (1994, 1997) evaluated the performance of two one-dimensional groundwater models, *viz.* a transfer function model (Box *et al.*, 1994), and SWATRE (Feddes *et al.*,1978; Belmans *et al.*, 1983). The first is an empirical model, while the latter is more physical-mechanistic in nature. Both models were equipped with an additive noise model. Therefore, in addition to a more detailed description of groundwater dynamics (also extreme values can be simulated), they also provide valuable information on the accuracy obtained. Although SWATRE performed slightly better in their case study, it required a lot of additional information on soil properties and drainage conditions.

Both physical-mechanistic and empirical models have their pros and cons. Empirical models are relatively fast, robust, need smaller amounts of data, and are less complicated than physical-mechanistic models. Physical-Mechanistic models on the other hand are less prone to extrapolation errors than empirical models due to their soil physical background. In this report, EMERALD is introduced, a stochastic hydrologic model in which the advantages of empirical and physical-mechanistic models are united. EMERALD is a physical-mechanistic model equipped with a stochastic component. In contrast with SWATRE, the soil-groundwater system is modelled by means of simple analytical expressions. As a result, EMERALD is more robust, requires less CPU-time, and erroneous results are easier to trace back. Another difference with both SWATRE and the transfer function-noise model is the way in which noise is added to the system. Noise can not only be added *a posteriori* to the deterministic model output, but can also serve as additional input to the groundwater system, where it is moulded by the physical-mechanistic analytical groundwater model. The resulting noise has therefore gained some colour, and contains site specific hydrological information. This latter property makes the noise, at least theoretically, transferable in space. We expect EMERALD to fill the gap between complex physical-mechanistic models and purely empirical models.

The outline of this report is as follows. In Chapter 2, we give the theoretical background of EMERALD. Each building stone of the model is addressed in detail. Chapter 3 is devoted to the calibration of the deterministic and stochastic components of EMERALD. The model is verified by means of simulation studies. The results of these studies are given in chapter 4. In chapter 5, EMERALD is confronted with real world data. Finally, the main conclusions are summarized in chapter 6.

2 Model description

In this chapter, the theoretical background of EMERALD is given. A schematic representation of the soil-groundwater system to be modelled is depicted in Fig. 2.1. Three subsystems can be distinguished, *i.e.* the root zone, the percolation zone, and the groundwater system. Each subsystem is successively addressed below.

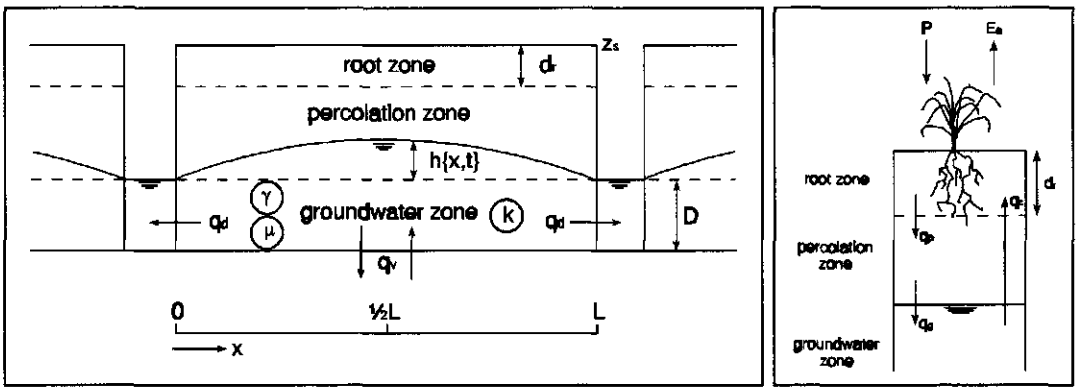

Fig. 2.1: Left: Schematic representation of the hydrologic system under study, showing fluxes of the saturated zone. Right: Enlargement of the figure on the left, showing fluxes in the unsaturated zone. The symbols are explained in the text, and in the list of symbols.

2.1 Root zone

The root zone is modelled as a nonlinear reservoir, *i.e.* its outflow is nonlinearly related to its moisture volume. The root zone is schematically depicted in Fig. 2.2.

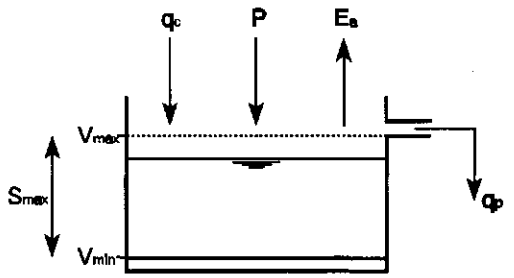

Fig. 2.2: Schematic representation of the root zone

Incoming fluxes are precipitation and capillary rise, outgoing fluxes are evapotranspiration and percolation. The volume of soil moisture in the root zone during time step t_k is obtained by solving the following water balance:

$$V(t_k) = V(t_{k-1}) + \left(P(t_k) + q_c(t_k) - E_a(t_k) - q_p(t_k)\right)\Delta t \qquad (2.1)$$

where

t_k = time step k [t];
V = volume of soil moisture in the root zone [L];
Δt = duration of time step t_k [t];
P = precipitation [Lt^{-1}];
E_a = actual evapotranspiration [Lt^{-1}];
q_c = capillary rise [Lt^{-1}];
q_p = percolation [Lt^{-1}]

The upper and lower bounds of V are governed by the soil moisture content at field capacity and wilting point respectively:

$$V_{max} = d_r \theta_{fc} \tag{2.2}$$

$$V_{min} = d_r \theta_{wp} \tag{2.3}$$

where

V_{max} = maximum volume of soil moisture in the root zone [L];
V_{min} = minimum volume of soil moisture in the root zone [L];
θ_{fc} = soil moisture content at field capacity [-];
θ_{wp} = soil moisture content at wilting point [-];
d_r = effective rooting depth [L]

The effective rooting depth is defined as the soil depth where just enough roots are available to entirely deplete the soil moisture storage capacity S_{max} (Wiersum & Reijmerink, 1990). S_{max} is given by:

$$S_{max} = V_{max} - V_{min} \tag{2.4}$$

Wiersum & Reijmerink (1990) also give a more practical definition of effective rooting depth: that level above which 90 percent of the roots are present.

In the following subsections, the components of the water balance are addressed.

2.1.1 Precipitation and evapotranspiration

The Royal Netherlands Meteorological Institute (KNMI) maintains an extensive monitoring network of meteorological stations. At these stations several meteorologic quantities are recorded or deduced. Among these are precipitation amounts and Makkink's reference-crop evapotranspiration. The latter corresponds to the evapotranspiration of an extensive area, uniformly covered with dry "standard" grass, 8-15 cm in height, and well supplied with water (CHO, 1986; Feddes, 1987). The potential evapotranspiration for other crops can be obtained by multiplying Makkink's reference-crop evapotranspiration E_r by a crop specific factor f_c:

$$E_p = f_c E_r \tag{2.5}$$

where

E_p = potential evapotranspiration [Lt^{-1}];
f_c = crop factor [-];
E_r = Makkink's reference-crop evapotranspiration [Lt^{-1}]

Feddes (1987) provides crop factors for several crops. By definition, the crop factor equals unity for "standard" grass. In case of soil moisture deficiencies, actual evapotranspiration is less than potential evapotranspiration, and is given by:

$$E_a = \alpha_s E_p \tag{2.6}$$

Reduction factor α_s is related to pressure head h_p. This relationship is completely defined by two parameters, *i.e.* limiting point and wilting point (Fig. 2.3). It bears some resemblance to the reduction function of Feddes *et al.* (1978), which relates actual to potential *trans*piration.

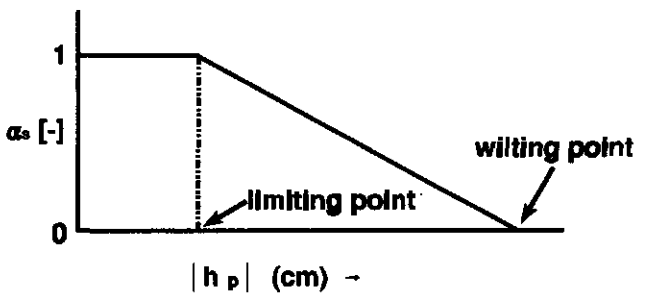

Fig. 2.3: Evapotranspiration reduction function

Pressure head is dependent on the moisture content of the root zone, according to (Wösten *et al.*, 1994):

$$h_p = \frac{1}{\alpha}\left(\left(\frac{\theta - \theta_r}{\theta_s - \theta_r}\right)^{\frac{n}{1-n}} - 1\right)^{\frac{1}{n}} \tag{2.7}$$

where θ is the moisture content [-], and θ_r [-], θ_s [-], α [L^{-1}], and n [-] are the Van Genuchten parameters. The Van Genuchten parameters for several representative soils in the Netherlands are tabulated in Wösten *et al.* (1994). The moisture content of the root zone can be obtained by:

$$\theta = \frac{V(t_{k-1})}{d_r} \tag{2.8}$$

So, having obtained the soil moisture content by means of Eq.2.8, the actual evapotranspiration can be computed by applying Eqs 2.7, 2.5, and 2.6 respectively.

2.1.2 Capillary rise

The amount of capillary rise reaching the root zone is governed by both groundwater depth, and the moisture content of the root zone. Capillary rise occurs if and only if the following condition is met:

$$V(t_{k-1}) + (P(t_k) - E_a(t_k))\Delta t < V_{max} \tag{2.9}$$

The maximum (or potential) amount of capillary rise is related to groundwater depth, and is modelled by a logistic function:

$$q_c^{max} = \frac{S_{max}}{\Delta t}\left(1 - \frac{1}{1 + \exp(b_0 + b_1 z)}\right) \tag{2.10}$$

This function and its parameters are graphically depicted in Fig. 2.4.

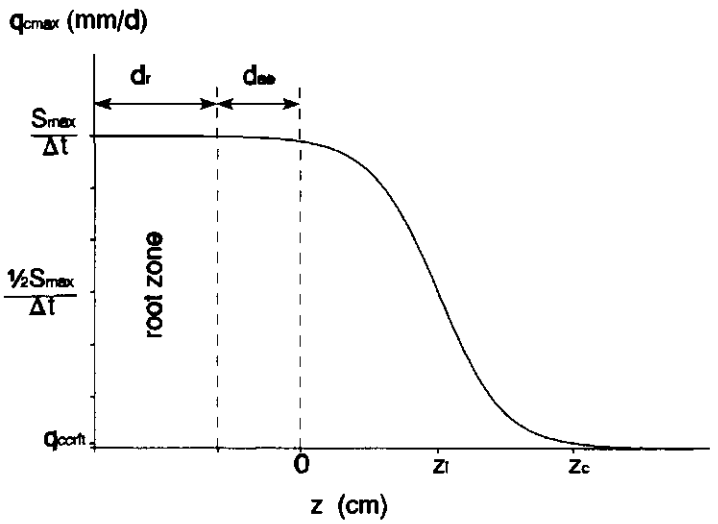

Fig. 2.4: Logistic function to model q_c^{max} as a function of z

Variable z is given by:

$$z = z_s - d_r - d_{ae} - h(t_{k-1}) \tag{2.11}$$

where

z_s = ground level with respect to drainage base [L];
d_r = effective rooting depth [L];
d_{ae} = thickness of the capillary fringe [L], *i.e.* the saturated zone above the groundwater table where the absolute value of the pressure head is greater than the air-entry value of the largest pores. In this report, we follow Gehrels (1995) by assuming that the air-entry value directly below the root zone equals pF 1.3;
$h(t_{k-1})$ = groundwater level with respect to drainage base at t_{k-1} [L].

In agricultural water management the term critical depth is employed to indicate the position of the phreatic surface where it is just able to supply a flux of 1.5 à 2 mm/day to the bottom of the root zone (Van der Sluijs, 1990). Smaller fluxes result in crop deterioration due to moisture deficits.

Given the following conditions:

$$q_c^{max} = q_c^{crit} \qquad \text{if } z = z_c$$
$$q_c^{max} = \frac{\frac{1}{2}S_{max}}{\Delta t} \qquad \text{if } z = z_i = -\frac{b_0}{b_1} = \frac{1}{2}z_c \tag{2.12}$$

where

q_c^{crit} = critical capillary flux [Lt^{-1}], usually 1.5 à 2.0 mm/day
z_c = critical depth minus thickness capillary fringe [L];
z_i = point of inflection of the logistic function [L].

Eq. 2.10 can be solved for b_0 and b_1. This results in:

$$b_0 = \ln\left(\frac{S_{max}}{0.2\Delta t} - 1\right)$$
$$b_1 = -\frac{2b_0}{z_c} \tag{2.13}$$

Gehrels (1995) used a linear rather than a logistic function to model the maximum amount of capillary rise. In this report, however, it is assumed that the gradual behaviour of a logistic function better complies with reality.

The actual amount of capillary rise is finally determined by the degree of saturation of the root zone:

$$q_c(t_k) = \begin{cases} q_c^{max} & \text{if } V(t_{k-1}) + \left(P(t_k) - E_a(t_k) + q_c^{max}(t_k)\right)\Delta t \le V_{max} \\ \dfrac{V_{max} - \left(V(t_{k-1}) + \Delta t\left(P(t_k) - E_a(t_k)\right)\right)}{\Delta t} & \text{if } V(t_{k-1}) + \left(P(t_k) - E_a(t_k) + q_c^{max}(t_k)\right)\Delta t > V_{max} \end{cases} \tag{2.14}$$

2.1.3 Percolation

Percolation occurs if field capacity is exceeded. In symbols:

$$V(t_{k-1}) + \left(P(t_k) - E_a(t_k)\right)\Delta t > V_{max} \tag{2.15}$$

The percolation flux is given by:

$$q_p(t_k) = \frac{V(t_{k-1}) + \left(P(t_k) - E_a(t_k)\right)\Delta t - V_{max}}{\Delta t} \tag{2.16}$$

2.2 Percolation zone

Two fluxes can be discerned in the percolation zone, *i.e.* an incoming and an outgoing flux (Fig. 2.1). The first, *i.e.* q_p, is the outgoing flux of the root zone, while the latter, *i.e.* groundwater recharge q_g, serves as input to the groundwater system. q_p does not instantaneously affect groundwater recharge, in fact the response of q_g is more or less delayed. Furthermore, as a result of storage and dispersion, q_g has a smoother appearance than q_p. Delay and smoothing are more pronounced in thick percolation zones. In section 2.2.1 an expression is derived to model both delay and smoothing for a single soil layer. In section 2.2.2 this expression is extended to the multi-layer case. Incorporation of preferential flow is discussed in section 2.2.3.

2.2.1 Single layer percolation zone

Delay and smoothing can be modelled by:

$$q_g(t_k) = \sum_{i=1}^{k} q_p(t_i)\, U_p(\Delta t, t_{k-(i-1)}) \tag{2.17}$$

where

q_g = groundwater recharge [Lt^{-1}];
q_p = percolation [Lt^{-1}];
U_p = pulse response of the percolation zone [-]

This expression gives groundwater recharge as the convolution of percolation and pulse response. The concept of pulse response stems from systems analysis. The pulse response of a system is defined as the response of the system to an input of unit volume occurring at a uniform rate for a period Δt (Dooge, 1973, p.127). Likewise, the pulse response in Eq.2.17 describes groundwater recharge as a function of time, resulting from a unit depth of percolation entering the percolation zone uniformly during time step Δt.

The pulse response is given by:

$$U_p(\Delta t, t) = S_p(t) - S_p(t-\Delta t) \tag{2.18}$$

where
$S_p(\cdot)$ = step response or S-curve for the percolation zone [-].

The step response of a system is defined as the output of the system resulting from zero input for $t<0$, and an input of unit intensity for $t\geq 0$ (cf. Dooge, 1973, p.86). In order to normalize the volume of the pulse response, Eq.2.18 is usually divided by Δt (see Dooge, 1973, p.86). In our case, however, normalization is inappropriate, since percolation is given as an intensity rather than a depth.

In short, Eq.2.17 can be applied if we are able to find an expression for either the pulse response or the step response. The latter can be derived by considering Richards' equation as a starting point. Richards' equation describes one-dimensional unsaturated flow in soil, and is given by (*e.g.* Koorevaar *et al.*, 1983):

$$\frac{\partial \theta}{\partial t} = \frac{\partial}{\partial z} k \left(\frac{\partial h_p}{\partial z} + 1 \right) \tag{2.19}$$

where
θ = soil moisture content [-];
t = time [t];
k = hydraulic conductivity [Lt^{-1}];
h_p = pressure head of soil moisture [L];
z = vertical space coordinate [L].

It can be derived by substituting Darcy's law, *i.e.*

$$q_z = -k \left(\frac{\partial h_p}{\partial z} + 1 \right) \tag{2.20}$$

into the equation of continuity, *i.e.*

$$\frac{\partial \theta}{\partial t} = -\frac{\partial q_z}{\partial z} \tag{2.21}$$

where q_z is the flux density in vertical direction. Since Eq.2.17 does only apply to linear systems, Richards' equation has to be linearized:

$$\frac{\partial q_z}{\partial t} = k'(\theta_{eff}) \frac{\partial q_z}{\partial z} + k(\theta_{eff}) h_p'(\theta_{eff}) \frac{\partial^2 q_z}{\partial z^2} \tag{2.22}$$

where

q_z = flux density in z-direction [Lt^{-1}];
t = time [t];
z = depth [L] (z is decreasing in downward direction);
$k(\theta_{eff})$ = hydraulic conductivity corresponding to θ_{eff} (see below) [Lt^{-1}];

and

$$k'(\theta_{eff}) = \left.\frac{\partial k}{\partial \theta}\right|_{\theta_{eff}} \qquad h_p'(\theta_{eff}) = \left.\frac{\partial h_p}{\partial \theta}\right|_{\theta_{eff}}$$

where

k = hydraulic conductivity [Lt^{-1}];
h_p = pressure head [Lt^{-1}]
θ = soil moisture content [-];
θ_{eff} = effective soil moisture content, *i.e.* the soil moisture content that corresponds to the mean vertical flux density [-].

It's derivation is given in Zwamborn (1995) and in annex 1. Eq.2.22 has the same form as the convection-dispersion equation used in solute transport. The analytical solution of the convection-dispersion equation for a step input, *i.e.* the step response of the system, is given by Bear (1979, p.268). Since $k'(\theta_{eff})$ corresponds to the convection parameter, and $k(\theta_{eff})h_p'(\theta_{eff})$ to the dispersion parameter this solution can be written as:

$$S_p(\bar{d}_p,t) = \frac{1}{2}\left[\operatorname{erfc}\left(\frac{\bar{d}_p - k'(\theta_{eff})t}{2\sqrt{k(\theta_{eff})h_p'(\theta_{eff})t}}\right) + \exp\left(\frac{k'(\theta_{eff})\bar{d}_p}{k(\theta_{eff})h_p'(\theta_{eff})}\right)\operatorname{erfc}\left(\frac{\bar{d}_p + k'(\theta_{eff})t}{2\sqrt{k(\theta_{eff})h_p'(\theta_{eff})t}}\right)\right] \tag{2.23}$$

Note that z has been replaced by $\bar{d}_p$, *i.e.* the average thickness of the percolation zone. The pulse response can now be obtained by applying Eq.2.18. Convolution of percolation and pulse response finally gives groundwater recharge (Eq.2.17).

2.2.2 Multi-layer percolation zone

It is often possible to discern more than one soil layer in the percolation zone, each with its own hydrological properties. In order to model a multi-layer percolation zone, Eq.2.17 should be generalized as follows:

$$q_j(t_k) = \sum_{i=1}^{k} q_{j-1}(t_i) U_{p_j}(\Delta t, t_{k-(i-1)}) \qquad \text{for } j=1,2,...,n_L \tag{2.24}$$

where

q_j = outflow of layer j [Lt^{-1}];
q_{j-1} = outflow of layer j-1 [Lt^{-1}];
U_{p_j} = pulse response for layer j of the percolation zone [-];
n_L = number of layers in the percolation zone [-].

Note that q_0 corresponds to q_p, and q_{n_L} to q_g.

2.2.3 Preferential flow

In practice, Richards' equation sometimes tends to overestimate delay. The reason is that through burrowing activities of soil animals, and by the presence of root channels and vertical cracks, part of the water entering the percolation zone reaches the groundwater faster than predicted. This preferential flow, or bypass flow as it is also called, can be modelled by:

$$q_j(t_k) = \sum_{i=1}^{k} (1-f_{b,j}) q_{j-1}(t_i) U_{p_j}(\Delta t, t_{k-(i-1)}) + f_{b,j} q_{j-1} \qquad \text{for } j=1,2,...,n_L \tag{2.25}$$

where $f_{b,j}$ is the fraction of preferential flow for subsoil layer j.

2.3 Groundwater system

The groundwater system is modelled by means of an analytical solution of the transient flow equation. Its derivation is given in section 2.3.1. On the basis of this solution, the step and pulse responses of the system are derived (sections 2.3.2 and 2.3.3). The latter is convolved with the net input to the groundwater system to obtain groundwater depth. In the final section, this convolution is rewritten in order to increase computational efficiency.

2.3.1 Transient flow equation

Groundwater flow is considered to be one-dimensional through a homogeneous unconfined aquifer. The groundwater system is schematically depicted in Fig. 2.1. Flow is subjected to the Dupuit-Forcheimer assumption, *i.e.* flow is horizontal, and its velocity uniform with depth. Furthermore $h \ll D$, and the saturated hydraulic conductivity k is assumed to be a constant. For these conditions, Darcy's law and the equation of continuity for horizontal saturated transient, *i.e.* time dependent, flow are given by Eqs 2.26 and 2.27 respectively (Dooge, 1973):

$$q_x = -kD\frac{\partial h}{\partial x} \tag{2.26}$$

$$\frac{\partial q_x}{\partial x} = q_n(t) - \mu\frac{\partial h}{\partial t} \tag{2.27}$$

where

q_x = flux density in x-direction (horizontal flow) [L^2t^{-1}];
q_n = net input to the groundwater system [Lt^{-1}];
D = effective drainage depth [L];
μ = specific yield [-];
t = time [t];
k = hydraulic conductivity [Lt^{-1}];
h = hydraulic head [L];
x = horizontal space coordinate [L].

Net input to the groundwater system q_n is defined as:

$$q_n = q_g + q_v - q_c \tag{2.28}$$

where

q_g = groundwater recharge [Lt^{-1}];
q_v = seepage ($q_v>0$) or infiltration ($q_v<0$) [Lt^{-1}];
q_c = capillary rise [Lt^{-1}].

Substituting Eq.2.26 into Eq.2.27 yields the one-dimensional transient flow equation:

$$kD\frac{\partial^2 h}{\partial x^2} + q_n(t) = \mu\frac{\partial h}{\partial t} \tag{2.29}$$

Kraijenhoff van de Leur (1958) derived its analytical solution subject to the initial and boundary conditions in Table 2.1:

$$h(x,t) = \frac{4q_n}{\pi\mu} J \sum_{n=1,3,5}^{\infty} n^{-3}\left[1 - \exp\left(-\frac{n^2 t}{J}\right)\right]\sin\left(\frac{n\pi x}{L}\right) \tag{2.30}$$

where L is the average distance between water courses (Fig. 2), and J (dimension: [t]) is given by:

$$J = \frac{\mu L^2}{\pi^2 kD} \tag{2.31}$$

Table 2.1: initial and boundary conditions to solve the transient flow equation

time	place	state	description
$t<0$	$0\le x\le L$	$q_n=0$	no input for $t<0$
$t\ge 0$	$0\le x\le L$	q_n=constant	constant input for $t\ge 0$
$t=0$	$0\le x\le L$	$h=0$	flat initial groundwater surface
$t\ge 0$	$x=0$	$h=0$	constant water level in water course at $x=0$
$t\ge 0$	$x=L$	$h=0$	constant water level in water course at $x=L$
$t\to\infty$	$0\le x\le L$	$\partial h/\partial t=0$	steady state (net input = groundwater discharge)

Reservoir characteristic J is related to drainage resistance, a more familiar parameter in Dutch water management. Drainage resistance is defined as the quotient of convexity and specific groundwater discharge during steady state conditions (CHO, 1986). In symbols:

$$\gamma = \frac{h(x=\tfrac{1}{2}L,\, t\to\infty)}{q_d} \tag{2.32}$$

Convexity at $t\to\infty$ (steady state) is given by:

$$\begin{aligned} h(x=\tfrac{1}{2}L,\, t\to\infty) &= \lim_{t\to\infty}\left\{\frac{4\,q_n}{\pi\mu}J\sum_{n=1,3,5}^{\infty} n^{-3}\left[1-\exp\left(\frac{-n^2t}{J}\right)\right]\sin\left(\frac{n\pi}{2}\right)\right\} \\ &= \frac{4q_n}{\pi\mu}J\sum_{n=1,-3,5,-7}^{\infty} n^{-3} \\ &= \frac{4q_nL^2}{\pi^3kD}\frac{\pi^3}{32} \\ &= \frac{L^2}{8kD}q_n \end{aligned} \tag{2.33}$$

At steady state, $q_d=q_n$. Hence, drainage resistance is given by:

$$\begin{aligned} \gamma &= \frac{h(x=\tfrac{1}{2}L,\, t\to\infty)}{q_d} \\ &= \frac{h(x=\tfrac{1}{2}L,\, t\to\infty)}{q_n} \\ &= \frac{L^2}{8kD} \end{aligned} \tag{2.34}$$

Combining Eqs.2.31 and 2.34 yields:

$$J = \frac{8\mu}{\pi^2}\gamma \tag{2.35}$$

Substituting Eq.2.35 into Eq.2.30 gives the solution of Kraijenhoff van de Leur in terms of drainage resistance:

$$h(x,t) = \frac{32q_n}{\pi^3}\gamma \sum_{n=1,3,5}^{\infty} n^{-3}\left[1 - \exp\left(\frac{-n^2\pi^2 t}{8\mu\gamma}\right)\right] \sin\left(\frac{n\pi x}{L}\right) \tag{2.36}$$

2.3.2 Flow as step response

Starting with an initial horizontal groundwater surface, Eq.2.36 describes the position of the phreatic surface as a function of space and time, resulting from a constant input q_n. If this input equals unity, Eq.2.36 gives the step response of the system:

$$S_h(x,t) = \frac{32}{\pi^3}\gamma \sum_{n=1,3,5}^{\infty} n^{-3}\left[1 - \exp\left(\frac{-n^2\pi^2 t}{8\mu\gamma}\right)\right] \sin\left(\frac{n\pi x}{L}\right) \tag{2.37}$$

In the previous section, specific groundwater discharge q_d was introduced in order to derive an expression for drainage resistance. By considering the definition of q_d as a starting point, its step response can be derived. Specific groundwater discharge is defined as the volume of groundwater discharge per unit of catchment area (CHO, 1986). In symbols:

$$q_d = \frac{q_s}{\frac{1}{2}L} \tag{2.39}$$

where q_s is the discharge per unit length of water course at x=0 or x=L [L^2t^{-1}]. This quantity can be obtained by evaluating Dupuit-Darcy at x=0 (or equivalently at x=L):

$$q_s = -kD\frac{\partial h}{\partial x}\bigg|_{x=0} \tag{2.40}$$

If the net input to the groundwater system equals unity, Eq.2.40 can be written as:

$$q_s = -kD\frac{\partial S_h}{\partial x}\bigg|_{x=0}$$

$$= -kD\frac{32}{\pi^3}\gamma\left\{\sum_{n=1,3,5}^{\infty} n^{-3}\left[1-\exp\left(-\frac{n^2\pi^2 t}{8\mu\gamma}\right)\right]\frac{n\pi}{L}\cos\left(\frac{n\pi x}{L}\right)\right\}_{x=0} \tag{2.41}$$

$$= -kD\frac{32}{\pi^2 L}\gamma\sum_{n=1,3,5}^{\infty} n^{-2}\left[1-\exp\left(-\frac{n^2\pi^2 t}{8\mu\gamma}\right)\right]$$

The step response of q_d can be obtained by substituting Eq.2.41 into Eq.2.39. Transmissivity kD can be eliminated by means of Eq.2.34:

$$S_{q_d}(t) = \frac{8}{\pi^2}\sum_{n=1,3,5}^{\infty} n^{-2}\left[1-\exp\left(-\frac{n^2\pi^2 t}{8\mu\gamma}\right)\right] \tag{2.42}$$

2.3.3 Flow as pulse response

In the previous section it was assumed that groundwater input q_n is invariant with time. However, since q_n is a function of time-dependent processes, like precipitation and evapotranspiration, this assumption does generally not hold. Precipitation and evapotranspiration are usually recorded on a daily basis, and can therefore be considered as pulses, *i.e.* average inputs during a given time step, in this case 1 day. Consequently, we need pulse responses rather than step responses. As was shown in section 2.2 the pulse response for time step Δt can be obtained by applying:

$$U(\Delta t,t) = S(t) - S(t-\Delta t) \tag{2.43}$$

Substitution of Eqs 2.37 and 2.42 into Eq.2.43 respectively gives:

$$U_h(x,\Delta t,t) = \frac{32}{\pi^3}\gamma\sum_{n=1,3,5}^{\infty} n^{-3}\left[\exp\left(\frac{n^2\pi^2\Delta t}{8\mu\gamma}\right)-1\right]\exp\left(-\frac{n^2\pi^2 t}{8\mu\gamma}\right)\sin\left(\frac{n\pi x}{L}\right) \tag{2.44}$$

$$U_{q_d}(\Delta t,t) = \frac{8}{\pi^2}\sum_{n=1,3,5}^{\infty} n^{-2}\left[\exp\left(\frac{n^2\pi^2\Delta t}{8\mu\gamma}\right)-1\right]\exp\left(-\frac{n^2\pi^2 t}{8\mu\gamma}\right) \tag{2.46}$$

Let $q_n(t_i)$ denote the average net input to the groundwater system during time step $(t_{i-1},t_i]$. The groundwater level at time t_k can then be obtained by convolution of q_n and U_h:

$$h(x,t_k) = \sum_{i=1}^{k} q_n(t_i)\, U_h(x,\Delta t,t_{k-(i-1)}) \tag{2.47a}$$

The specific groundwater discharge can be obtained in a similar way:

$$q_d(t_k) = \sum_{i=1}^{k} q_n(t_i)\, U_{q_d}(\Delta t, t_{k-(i-1)}) \tag{2.49a}$$

These expressions are only valid in case the initial conditions in Table 2.1 are met, *i.e.* $h(x,t_0)=0\ \forall\ \{x \mid 0 \le x \le L\}$ and consequently $q_d(t_0)=0$. Otherwise, a correction term should be added to each expression (*e.g.* De Zeeuw, 1966):

$$h(x,t_k) = h(x,t_0)\exp\left(-\frac{t_k\pi^2}{8\mu\gamma}\right) + \sum_{i=1}^{k} q_n(t_i)\, U_h(x,\Delta t, t_{k-(i-1)}) \tag{2.47b}$$

$$q_d(t_k) = q_d(t_0)\exp\left(-\frac{t_k\pi^2}{8\mu\gamma}\right) + \sum_{i=1}^{k} q_n(t_i)\, U_{q_d}(\Delta t, t_{k-(i-1)}) \tag{2.49b}$$

In this report, however, the correction terms are omitted because their contribution to the total expressions diminishes quickly as t_k increases.

2.3.4 Time series representation

In order to increase computational efficiency, Eqs 2.47a and 2.49a are rewritten according to the day-by-day method of De Zeeuw (1966). This method leads to the following recurrence relations (Annex 2) if the higher order terms are neglected:

$$h(t_k) = \delta h(t_{k-1}) + \omega_0 q_n(t_k) + \omega_1 q_n(t_{k-1}) \tag{2.50}$$

$$q_d(t_k) = \delta q_d(t_{k-1}) + \omega_0' q_n(t_k) + \omega_1' q_n(t_{k-1}) \tag{2.51}$$

where

$$\delta = \exp\left(-\frac{\Delta t\pi^2}{8\mu\gamma}\right)$$

$$\omega_0 = \frac{32}{\pi^3}\gamma(1-\delta)\sin\left(\frac{\pi x}{L}\right) + \Delta U_h(1)$$

$$\omega_1 = -\delta\Delta U_h(1)$$

$$\omega_0' = \frac{8}{\pi^2}(1-\delta) + \Delta U_{q_d}(1)$$

$$\omega_1' = -\delta\Delta U_{q_d}(1)$$

$$\Delta U_h(1) = \frac{32}{\pi^3}\gamma\sum_{n=3,5,7}^{\infty} n^{-3}\left(1-\delta^{n^2}\right)\sin\left(\frac{n\pi x}{L}\right)$$

$$\Delta U_{q_d}(1) = \frac{8}{\pi^2}\sum_{n=3,5,7}^{\infty} n^{-2}\left(1-\delta^{n^2}\right)$$

Parameter δ is the autoregressive parameter of the model, and ω_0, ω_1, ω_0' and ω_1' are its moving average parameters.

In case of capillary rise, $q_n(t_k)$ is a function of $h(t_k)$. Therefore, Eqs 2.50 and 2.51 are nonlinear. A linear approximation can be obtained by letting $q_n(t_k)$ depend on $h(t_{k-1})$:

$$h(t_k) \approx \delta h(t_{k-1}) + \omega_0 q_n(t_k, h(t_{k-1})) + \omega_1 q_n(t_{k-1}, h(t_{k-2})) \tag{2.52}$$

$$q_d(t_k) \approx \delta q_d(t_{k-1}) + \omega_0' q_n(t_k, h(t_{k-1})) + \omega_1' q_n(t_{k-1}, h(t_{k-2})) \tag{2.53}$$

Eqs 2.52 and 2.53 represent the deterministic component of EMERALD. An important property of this component is that it incorporates hysteresis effects, a commonly observed feature of flood waves (*e.g.* Shaw, 1983). Two hysteresis loops are shown in Fig. 2.5, *i.e.* an exact solution and an approximation. The exact solution is computed by means of Eqs 2.47b and 2.49b. The approximation, on the other hand, is obtained by applying Eqs 2.52 and 2.53. It can be concluded that the assumption $\Delta U(i)=0$ for $i=2,3,...,\infty$ made in annex 2 does not significantly affect the results.

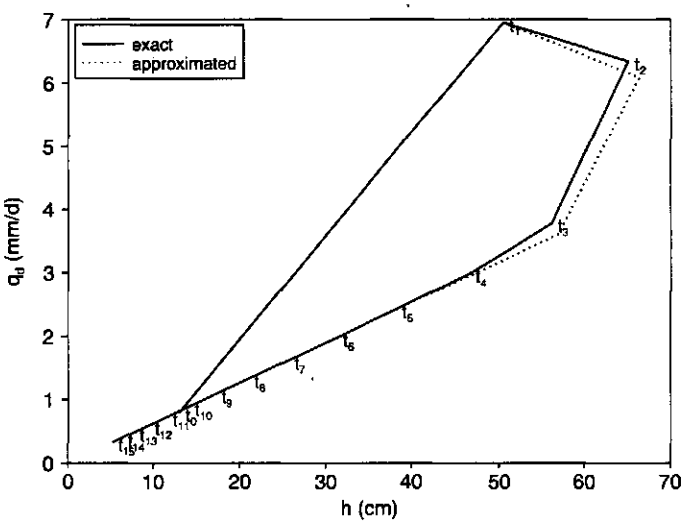

Fig. 2.5: Hysteresis loops according to the expression of Kraijenhoff van de Leur. The solid line is based on the exact solution, the dashed line on its approximation.

2.3.5 Incorporating uncertainty

In the previous sections, several simplification have been made to facilitate the derivation of EMERALD. These simplifications, together with uncertain model parameters and input, will finally lead to errors in the model output. It is assumed

that the deterministic component of EMERALD, once properly calibrated, offsets all systematic errors. In order to take random errors into account, a realization of noise process N is added to q_n, *i.e.* one of the most uncertain parameters of EMERALD. As a consequence q_n, and therefore h and q_d will become random variables. The stochastic counterparts of Eqs 2.52 and 2.53 are given by:

$$H(t_k) = \delta H(t_{k-1}) + \omega_0 Q_n(t_k, H(t_{k-1})) + \omega_1 Q_n(t_{k-1}, H(t_{k-2})) + \omega_0 N(t_k) + \omega_1 N(t_{k-1}) \quad (2.55)$$

$$Q_d(t_k) = \delta Q_d(t_{k-1}) + \omega_0' Q_n(t_k, H(t_{k-1})) + \omega_1' Q_n(t_{k-1}, H(t_{k-2})) + \omega_0' N(t_k) + \omega_1' N(t_{k-1}) \quad (2.56)$$

In the remaining chapters of this report, random variables will be expressed in uppercase.

There are many ways to model noise process N (*e.g.* Box *et al.*, 1994; Chatfield, 1989). In this report, it is modelled as a zero-mean autoregressive process of order 1:

$$N(t_k) = \phi N(t_{k-1}) + \varepsilon(t_k) \quad (2.57)$$

where
N = random error [Lt^{-1}];
ϕ = autoregressive parameter [-];
ε = discrete-time white noise [Lt^{-1}]

Discrete-time white noise has the following properties:

$$E\{\varepsilon(t_k)\} = 0 \quad (2.58)$$

$$Var\{\varepsilon(t_k)\} = E\{\varepsilon(t_k)^2\} = \sigma_\varepsilon^2 \quad (2.59)$$

$$Cov\{\varepsilon(t_k), \varepsilon(t_{k+\tau})\} = E\{\varepsilon(t_k)\varepsilon(t_{k+\tau})\} = 0 \quad \forall\ \tau \neq 0 \quad (2.60)$$

where
σ_ε^2 = variance of ε [L^2t^{-2}]
τ = lag [-]

Eqs 2.55 and 2.56 consist of a transfer function model (non-N-terms) and a noise model (N-terms). Unlike the models applied by Knotters & Van Walsum (1995, 1997) the noise is part of the model's input, and not added *a posteriori* to its deterministic output. In the remaining chapters of this report, the first type of noise is referred to as internal noise, while the second type is called external noise. EMERALD supports both internal and external noise models. The advantage of an internal noise model

is that not only H but also Q_d, E_a, E_p, V, Q_p, Q_g, Q_c and Q_n become stochastic. This means that they also incorporate model uncertainty. Moreover, both the transfer function model and the internal noise model contain site specific information, *i.e.* drainage resistance, specific yield and geographic position (x and L). This is a very powerful property since it makes the parameters of the model transferable in space. However, one critical comment should be made in this respect. The shape of the phreatic surface is often not parabolical as is assumed by the expression of Kraijenhoff van de Leur (Fig. 2.1), but more or less trapezoidal, with steep slopes near the drainage courses. This is especially true for sandy areas. In other words, groundwater fluctuation near drainage courses is for trapezoidal surfaces very similar to fluctuation near the centre of the plot, where x/L=0.5. Therefore, in case of trapezoidal groundwater surfaces, the ratio x/L near drainage courses should also be set to 0.5, or to some slightly smaller value. This implies that the model does no longer depend on the ratio x/L anymore.

2.4 Simulation and prediction

Eqs 2.55 and 2.56 can be used to generate realizations of time series of groundwater levels and specific groundwater discharge. The AR(1)-process N is given by:

$$N(t_k) = \phi N(t_{k-1}) + \sigma_\varepsilon Z \tag{2.61}$$

where Z is a normally distributed deviate with zero mean and unit variance (Z–$N(0,1)$).

Predictions can be obtained by taking the expected values of H and Q_d:

$$\mathrm{E}\{H(t_k)\} = \delta \mathrm{E}\{H(t_{k-1})\} + \omega_0 \mathrm{E}\{Q_n(t_k, H(t_{k-1}))\} + \omega_1 \mathrm{E}\{Q_n(t_{k-1}, H(t_{k-2})\} \tag{2.62}$$

$$\mathrm{E}\{Q_d(t_k)\} = \delta \mathrm{E}\{Q_d(t_{k-1})\} + \omega_0' \mathrm{E}\{Q_n(t_k, H(t_{k-1})\} + \omega_1' \mathrm{E}\{Q_n(t_{k-1}, H(t_{k-2})\} \tag{2.63}$$

In order to express these equations entirely in terms of expected values of H, it is assumed that:

$$\mathrm{E}\{Q_n(t_k, H(t_{k-1})\} \approx q_n(t_k, E\{H(t_{k-1})\}) \tag{2.64}$$

This assumption is legitimate as long as Q_n is linearly related to H. Since Q_n is only dependent on H by means of capillary rise, and since this dependency is modelled by a sigmoid function, this assumption is reasonable, except for the tails of this function. Eqs 2.62 and 2.63 can therefore be written as:

$$\mathrm{E}\{H(t_k)\} = \delta E\{H(t_{k-1})\} + \omega_0 q_n(t_k, E\{H(t_{k-1})\}) + \omega_1 q_n(t_{k-1}, E\{H(t_{k-2})\}) \tag{2.65}$$

$$E\{Q_d(t_k)\} = \delta E\{Q_d(t_{k-1})\} + \omega_0' q_n(t_k, E\{H(t_{k-1})\}) + \omega_1' q_n(t_{k-1}, E\{H(t_{k-2})\}) \tag{2.66}$$

Given the initial conditions $E\{H(t_0)\}$ and $E\{Q_d(t_0)\}$, these expressions can be used to predict groundwater levels and specific discharge. The prediction errors are given by:

$$H'(t_k) = H(t_k) - E\{H(t_k)\} \tag{2.67}$$

$$Q_d'(t_k) = Q_d(t_k) - E\{Q_d(t_k)\} \tag{2.68}$$

The variances of these errors are derived in annex 4, and read:

$$\mathrm{Var}\{H'(t_k)\} = \sigma_\varepsilon^2 \frac{(\omega_0^2 + \omega_1^2)(1 + \delta\phi) + 2\omega_0\omega_1(\delta + \phi)}{(1 - \phi^2)(1 - \delta\phi)(1 - \delta^2)} \tag{2.69}$$

$$\mathrm{Var}\{Q_d'(t_k)\} = \sigma_\varepsilon^2 \frac{(\omega_0'^2 + \omega_1'^2)(1 + \delta\phi) + 2\omega_0'\omega_1'(\delta + \phi)}{(1 - \phi^2)(1 - \delta\phi)(1 - \delta^2)} \tag{2.70}$$

3 Model calibration

Calibration takes place in two steps. First the deterministic component of EMERALD is calibrated (section 3.1). If the time series of observed groundwater depths is not affected by external trends, *i.e.* trends not induced by precipitation excess, calibration of the deterministic model should remove systematic errors in model output. Random errors are dealt with in the second calibration step. During this step the stochastic part of EMERALD is calibrated given the calibrated deterministic model of the first step. Three calibration methods for the stochastic component are given in section 3.2.

3.1 Calibration of the deterministic component

Three parameters of the deterministic component (Eq. 2.52) are considered for calibration, *i.e.* γ, μ and q_v. Calibration can be accomplished by minimizing the following objective function:

$$f_{obj}(\gamma, \mu, q_v) = \frac{1}{n_Y} \sum_{i=1}^{n_Y} [Y(t_i) - h(t_i)]^2 \tag{3.1}$$

where

Y = observed groundwater level [L];
h = groundwater level predicted by the deterministic component [L];
n_Y = number of observations [-].

Several optimization techniques are available for this purpose. We applied the Downhill Simplex method (Press *et al.*, 1989).

3.2 Calibration of the stochastic component

The calibrated deterministic component serves as a starting-point for the calibration of the stochastic component. The parameters to calibrate are ϕ and σ_ε^2. In this section, three calibration methods are discussed. Each method requires an equidistant time series of observed groundwater levels. In section 3.2.1 a method is given which uses $\mathrm{Cov}\{N(t_k),N(t_{k+\tau})\}$ to calibrate the parameters of an internal noise model. The remaining sections address two calibration methods which are based on $\mathrm{Cov}\{H'(t_k),H'(t_{k+\tau})\}$. The method in section 3.2.2 deals with internal noise, while the method in section 3.2.3 is appropriate for external noise.

3.2.1 Calibration of internal noise: the inverse model approach

The aim of this calibration method is to estimate parameters ϕ and σ_ε^2 of AR(1)-process N, that is added to the net input to the groundwater system (section 2.3.5). A time series of $\bar{N}$ *i.e.*, the average N over time step Δt_Y, can be obtained after rewriting Eq.2.55:

$$\bar{N}(t_k) = \omega_0^{-1}\left[Y(t_k) - \delta Y(t_{k-1}) - \omega_0 \bar{q}_n(t_k, h(t_{k-1})) - \omega_1 \bar{q}_n(t_{k-1}, h(t_{k-2})) - \omega_1 N(t_{k-1})\right] \tag{3.2}$$

where Y is the observed groundwater level [L]. The average net inputs $\bar{q}_n$ to the groundwater system can be computed by running the (calibrated) deterministic component of EMERALD for time step Δt, and averaging the resulting time series of $q_n(\Delta t)$ over Δt_Y.

The experimental autocovariance function of $\bar{N}$ can be estimated by:

$$\hat{C}(\Delta t_Y, \tau) = \frac{1}{n_Y - \tau}\sum_{i=1}^{n_Y-\tau} \bar{N}(t_i)\bar{N}(t_{i+\tau}) \tag{3.3}$$

where

n_Y = number of observations [-];

τ = lag [-]

The noise parameters for time step Δt=1 can now be obtained by fitting the theoretical autocovariance function to the experimental one. The theoretical autocovariance function is derived in annex 3, and reads:

$$\mathrm{Cov}\{\bar{N}(t_k), \bar{N}(t_{k+\tau})\} = \begin{cases} \dfrac{\sigma_\varepsilon^2}{(1-\phi^2)n^2}\displaystyle\sum_{i=0}^{n-1}\sum_{j=0}^{n-1}\phi^{|i-j|} & \text{for } \tau=0 \\ \dfrac{\sigma_\varepsilon^2}{(1-\phi^2)n^2}\phi^{n(\tau-1)+1}\left(\dfrac{1-\phi^n}{1-\phi}\right)^2 & \text{for } \tau>0 \end{cases} \tag{3.5}$$

where

ϕ = autoregressive parameter of the noise model for time step Δt=1 day [-];

σ_ε^2 = variance of noise model for time step Δt=1 day [L^2t^{-2}];

n = $\Delta t_Y/\Delta t$ where Δt=1 day [-].

3.2.2 Calibration of internal noise: the forward model approach

In this section, calibration is not based on the autocovariance function of N, but on the autocovariance function of the prediction errors of h. These errors are given by (cf. Eq.2.67):

$$H'(t_k) = Y(t_k) - h(t_k) \tag{3.6}$$

where
Y = observed groundwater level [L];
h = groundwater level obtained by the calibrated deterministic model [L].

The lag τ autocovariances pertaining to H' can be estimated by:

$$\hat{C}(\tau) = \frac{1}{n_Y - \tau}\sum_{i=1}^{n_Y-\tau} H'(t_i)H'(t_{i+\tau}) \tag{3.7}$$

In annex 4 the theoretical autocovariance function of $H'(t_k)$ is derived. It is given by:

$$\mathrm{Cov}\{H'_k, H'_{k+\tau}\} = \sigma_\varepsilon^2 \frac{(\omega_0^2+\omega_1^2)(\delta^{-\tau}+\phi\delta^{\tau+1}+\eta_1)+\omega_0\omega_1(\delta^{1-\tau}+\delta^{-1-\tau}+\phi\delta^{\tau}(1+\delta^2)+\eta_2+\eta_3)}{(1-\phi^2)(1-\delta\phi)(1-\delta^2)} \tag{3.8}$$

where

$$\eta_1 = \begin{cases} 0 & \text{for } \tau = 0 \\ \dfrac{1-\phi\delta}{1-\phi/\delta}\left(\delta^{\tau}-\phi^{\tau}\right)-\delta^{-\tau}+\phi^{\tau} & \text{for } \tau=1,2,\ldots,\infty \end{cases}$$

$$\eta_2 = \begin{cases} 0 & \text{for } \tau\in\{0,1\} \\ \dfrac{1-\phi\delta}{1-\phi/\delta}\left(\delta^{\tau-1}-\phi^{\tau-1}\right)-\delta^{1-\tau}+\phi^{\tau-1} & \text{for } \tau=2,3,\ldots,\infty \end{cases}$$

$$\eta_3 = \frac{1-\phi\delta}{1-\phi/\delta}\left(\delta^{\tau+1}-\phi^{\tau+1}\right)-\delta^{-\tau-1}+\phi^{\tau+1} \qquad \text{for } \tau=0,1,\ldots,\infty$$

Fitting the theoretical autocovariance function to the experimental autocovariances estimated by Eq.3.7 yields parameters ϕ and σ_ε^2.

3.2.3 Calibration of external noise: the forward model approach

This method is similar to that of Knotters & Van Walsum (1995, 1997). Instead of adding noise process N to q_n it is added to the output of the deterministic output h:

$$H(t_k) = h(t_k) + N(t_k) \tag{3.9}$$

Therefore, $N(t_k)$ can be estimated by:

$$N(t_k) = Y(t_k) - h(t_k) \tag{3.10}$$

The experimental autocovariance function of N can be estimated by:

$$\hat{C}(\tau) = \frac{1}{n_Y - \tau} \sum_{i=1}^{n_Y - \tau} N(t_i) N(t_{i+\tau}) \tag{3.11}$$

Note that $t_{i+\tau} - t_i = \tau \Delta t_Y$. The theoretical autocovariance function for an AR(1)-process is given by:

$$C(\tau) = \frac{\sigma_\varepsilon^2}{1 - \phi^2} \phi^{|\tau|} \tag{3.12}$$

Fitting this expression to the autocovariances computed by Eq.3.11 gives noise parameters ϕ and σ_ε^2.

Once the model is properly calibrated, simulation can be performed by adding realizations of N to the deterministic time series of h (Eq.2.57).

4 Model verification

In this chapter, some components of EMERALD are verified. Thorough testing of all ins and outs of program behaviour falls beyond the scope of this report. Only some limited testing has been performed to achieve some basic insights. The results should be considered as a guide line for further modelling and testing.
In section 4.1, the expression for estimating the variance of the prediction errors is verified. In section 4.2 the calibration method of the deterministic component of EMERALD is addressed. The chapter is concluded by testing the calibration methods of the stochastic components of EMERALD (section 4.3).

4.1 Variance of prediction errors

In section 2.4 an expression was given to estimate the variance of prediction errors of h (Eq.2.69). It was derived in annex 4 subject to the assumption that Q_n is independent of H. In practice, however, this assumption does generally not hold due to the occurrence of capillary rise. It is therefore interesting to test the validity of expression 2.69 in case capillary rise can not be ignored.

For this purpose, 1000 traces of 1 year were simulated for different drainage levels. This is analogous to simulating 1000 traces with different amounts of capillary rise. The following parameter values were used: ϕ=0.0, x/L=0.5, μ=0.2, γ=250 days, q_v=0 mm/d. In order to obtain σ_r^2, Eq.2.69 was solved for σ_r^2 after setting Var$\{H'\}$ equal to 200 cm^2. In addition, the soil characteristics of well 12BL0015 (Table 5.1), and the meteorologic data of 1982 of Eelde were used. In order to diminish the effect of initial values, a warming-up period of two years was considered. For each day Var$\{H'\}$ and E$\{Q_c\}$ were estimated for the ensemble of realizations. The results are shown in Fig. 4.1.

Figure 4.1 clearly illustrates the effects of capillary rise. When capillary rise is insignificant (z_0<-200 cm), Var$\{H'\}$ is estimated quite well. However, when the drainage level is increased, capillary rise becomes more pronounced and the estimate Var$\{H'\}$=200 cm^2 becomes biased. As z_0 further increases (z_0=-50 cm), all realizations contribute maximally and equally to capillary rise, and Var$\{H'\}$ is estimated well again.

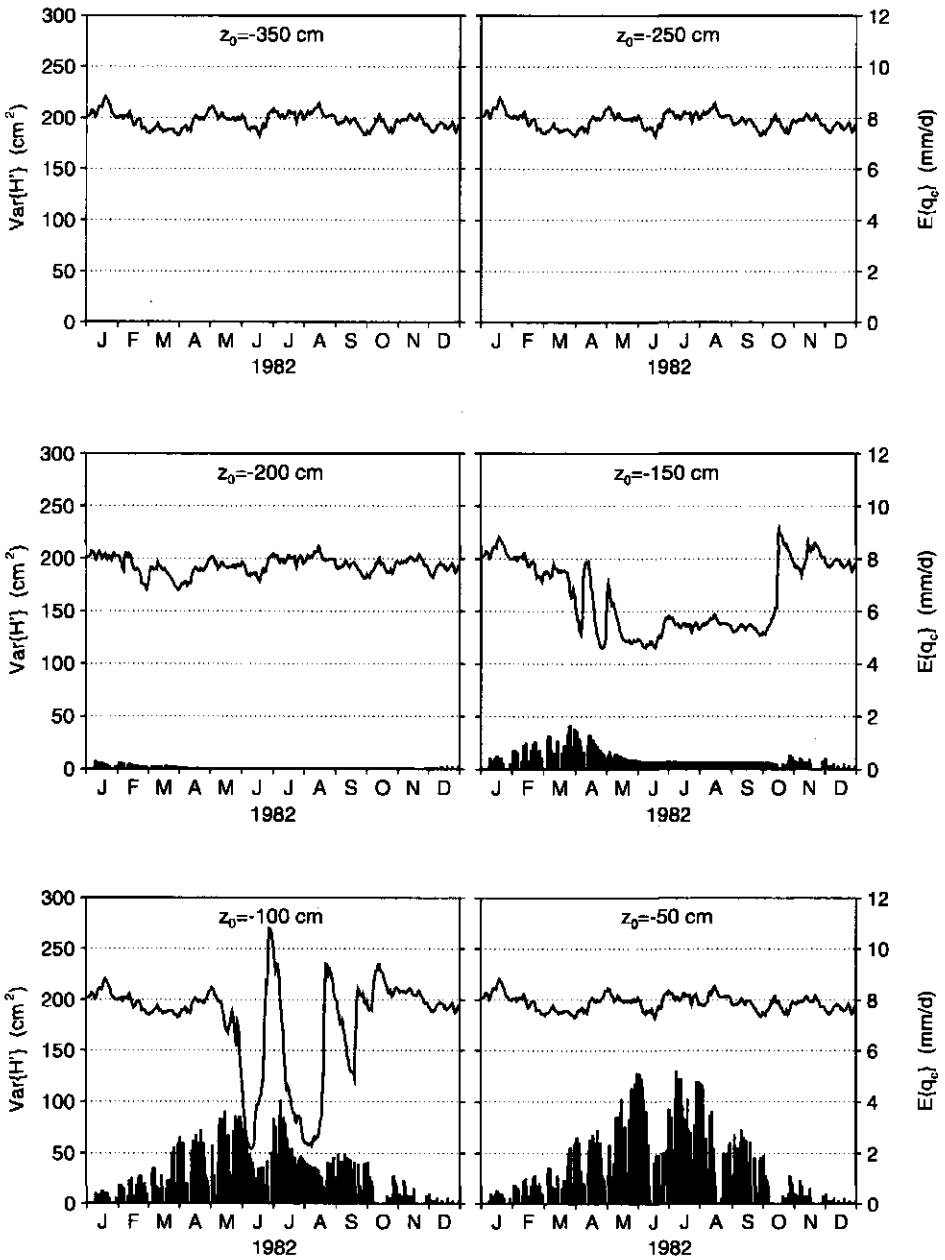

Fig. 4.1: Var{H'} (solid line) and E{Q_c} (bars), based on 1000 simulated traces of groundwater levels and capillary rise respectively. The position of drainage level z_0 is varied from 350 cm (upper left) to 50 cm below the soil surface (lower right). The variance of prediction errors of H equals 200 cm^2

4.2 Calibration of the deterministic component

The performance of the calibration method for the deterministic component was tested by means of Monte Carlo analysis. For four levels of Var{H'} and four time steps (Δt_Y), 100 synthetic time series of "observations" were generated by random selection of γ, μ, and q_v from uniform distributions. The parameter sets employed in this test are given in Table 4.1. Pedology and hydrology were adopted from well 12BL0015 (see Table 5.1). Furthermore, a warming-up period of two years was taken into account.

Table 4.1: Parameters applied in the Monte Carlo analysis

parameter	value(s)/range	selection
ϕ	0	fixed
Var{H'}	0,100,200,300 cm^2	alternating
Δt_Y	1,5,10,15 day(s)	alternating
μ	0.05 to 0.35	randomly
γ	10 to 750 days	randomly
q_v	-1 to 1 mm/d	randomly

Monte Carlo simulation resulted in a total of 1600 (4 times 4 times 100) synthetic time series of "observations", covering the 10-year period 1961-1970. Each time series was calibrated for γ, μ, and q_v. For each combination of Var{H'} and Δt_Y two verification measures were computed, *i.e.* the mean error (ME), and the root mean squared error (RMSE). These measures are given by:

$$\mathrm{ME} = \frac{1}{n}\sum_{i=1}^{n}(p_i - \hat{p}_i) \tag{4.1}$$

$$\mathrm{RMSE} = \sqrt{\frac{1}{n}\sum_{i=1}^{n}(p_i - \hat{p}_i)^2} \tag{4.2}$$

where

p_i = randomly selected parameter of interest (γ, μ, or q_v);

$\hat{p}_i$ = calibrated parameter of interest ($\hat{\gamma}$, $\hat{\mu}$, or $\hat{q}_v$);

n = number of realizations (n=100).

The results are given in Fig. 4.2. It can be concluded that the parameters of fully deterministic traces, *i.e.* Var{H'}=0, are estimated very well. In case Var{H'} increases from 100 cm^2 to 300 cm^2, the RMSE and the absolute value of the ME only increase slightly. In short, it can be concluded that the calibration procedure for the deterministic component works very well.

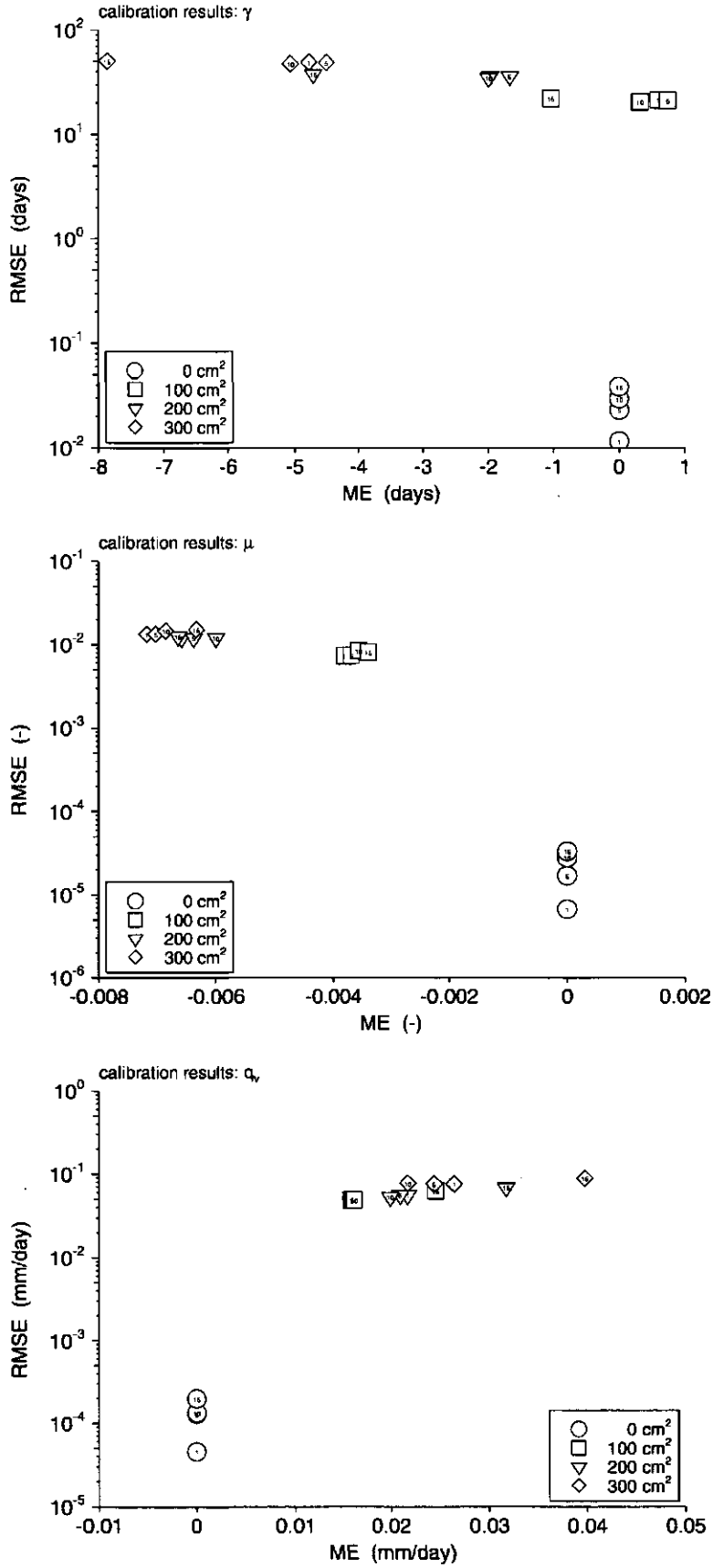

Fig. 4.2: MEs and RMSEs for 16 combinations of Var{H'} and Δt_γ. Variance levels are indicated by open symbols (circles, squares, triangles, and diamonds), time steps (in days) are printed at the centre of the symbols. From top to bottom, γ, μ, and q_v.

4.3 Calibration of the stochastic model

The performances of both internal noise calibration methods were tested. The method for calibrating external noise is left out of consideration, since similar procedures were already tested elsewhere (*e.g.* Knotters & Van Walsum, 1995). For 15 times 15 combinations of γ and Δt_Y, 100 realizations of time series of 10 and 30 years were simulated. The following parameters were kept constant: μ=0.20, ϕ=0.25, Var{H'}=200 cm^2. Pedology and hydrology were again adopted from well 12BL0015 (Table 5.1). Each of the simulated 45000 time series was calibrated for ϕ and σ_ε^2 according to the forward model approach (IF) and the inverse model approach (II). The estimates obtained by calibration, *i.e.* $\hat{\phi}$ and $\hat{\sigma}_\varepsilon^2$, were confronted with the parameters used for simulation *i.e.* ϕ and σ_ε^2. This was accomplished by comparing the first 10 lags of the autocovariance function based on ϕ and σ_ε^2 with those based on $\hat{\phi}$ and $\hat{\sigma}_\varepsilon^2$. Again, the ME and RMSE were used for this purpose:

$$\mathrm{ME} = \frac{1}{10}\sum_{\tau=0}^{9}\left(\hat{C}(\hat{\phi}, \hat{\sigma}_\varepsilon^2, \tau) - C(\phi, \sigma_\varepsilon^2, \tau)\right) \tag{4.3}$$

$$\mathrm{RMSE} = \sqrt{\frac{1}{10}\sum_{\tau=0}^{9}\left[\hat{C}(\hat{\phi}, \hat{\sigma}_\varepsilon^2, \tau) - C(\phi, \sigma_\varepsilon^2, \tau)\right]^2} \tag{4.4}$$

Finally, the expected values of the ME and RMSE for each combination of γ and Δt_Y were computed by taking their arithmetic averages over all realizations. The results are presented in Figures 4.3 and 4.4, both for the 10-year period and for the 30-year period. The 10-year period can be used to evaluate the performances of the calibration methods for situations commonly encountered in practice. The 30-year period should be considered as a reference situation, based on an almost exhaustive set of observations.

As expected, the performances of both methods decrease when Δt_Y increases. Performances also decrease when drainage resistance increases. This is due to the following reasons. First, the effect of capillary rise. As became clear in section 4.1, capillary rise significantly affects the accuracy Eq.2.69. This is also true for Eq.3.8 which is based on the same assumption. Large drainage resistances result in rapidly rising and slowly falling groundwater levels, and therefore in potentially greater amounts of capillary rise. This reduces the validity of Eq.3.8, and worsens the performance of the IF-method. Second, a larger drainage resistance corresponds to a larger memory of the system (larger autoregressive parameter). Hence, in order to obtain the same level of accuracy, a longer time-series of observations is required.

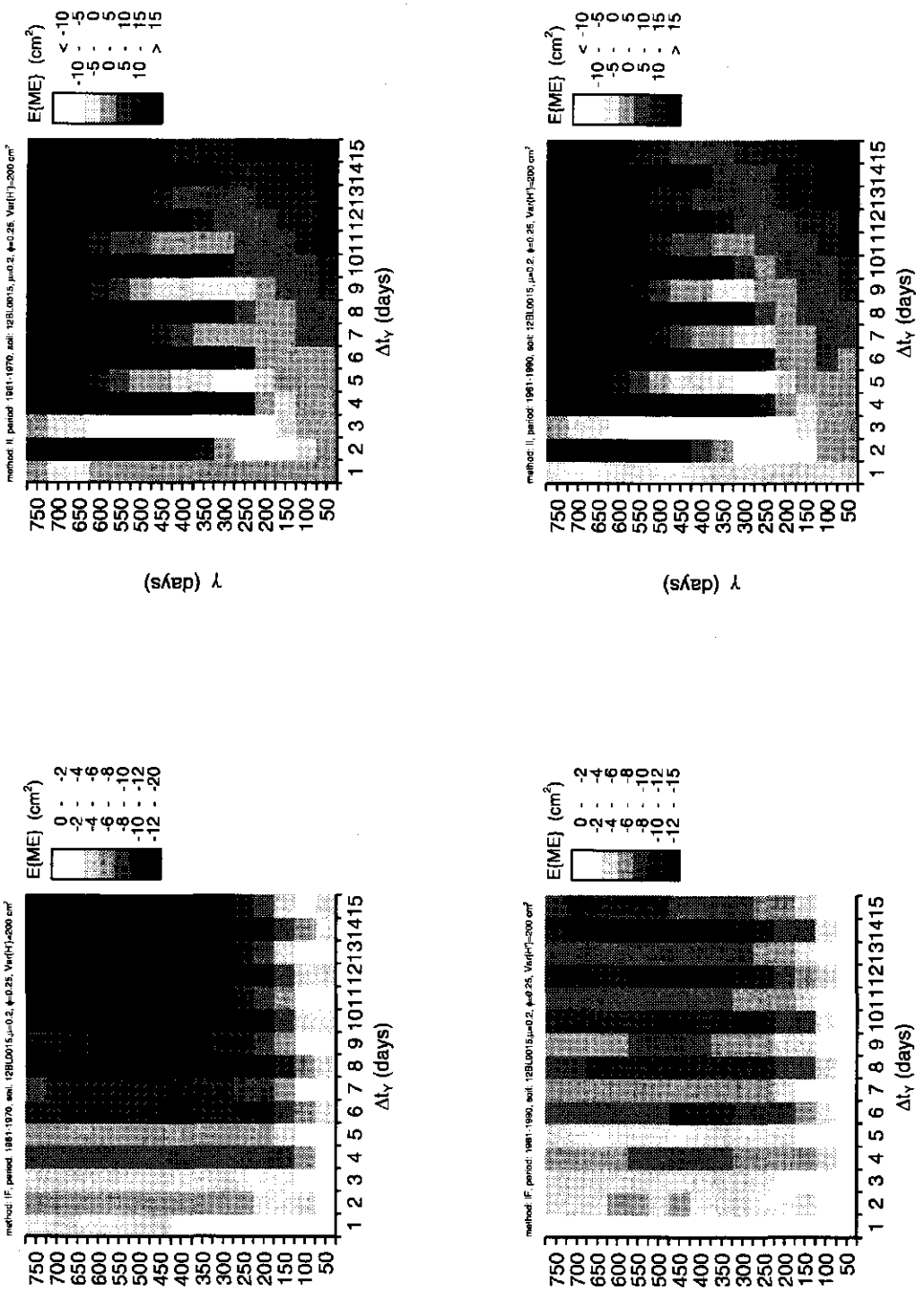

Fig. 4.3: Expected value of the ME for two calibration methods (IF and II) and two time spans (10 and 30 years) as a function of γ and Δt_γ

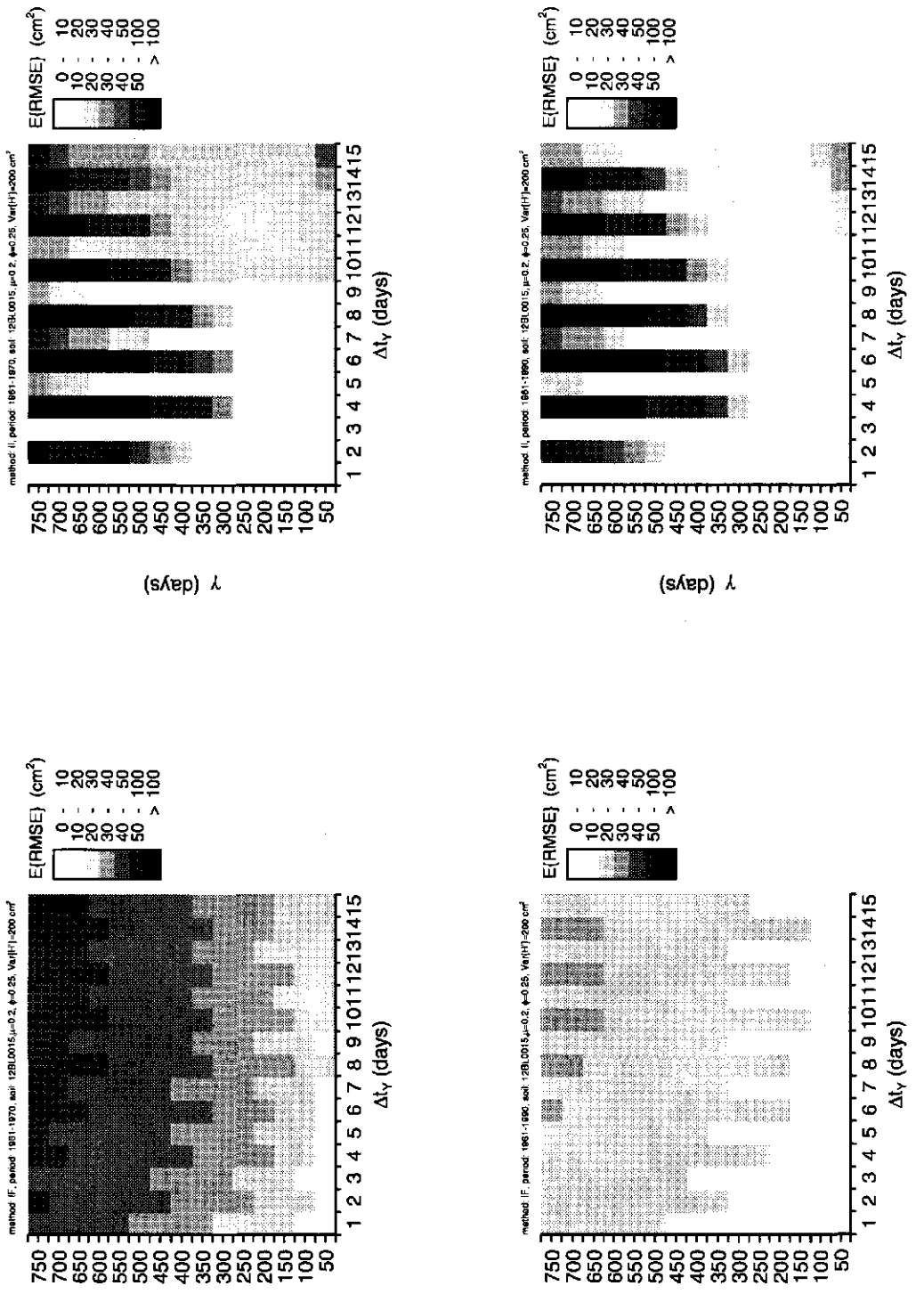

Fig. 4.4: Expected value of the RMSE for two calibration methods (IF and II) and two time spans (10 and 30 years) as a function of γ and Δt_γ

Very striking in Figs 4.3 and 4.4 are the vertical strips of alternating large and low E{ME}s and E{RMSE}s. At first glance, these results may look contradictory, as large Δt_Ys yield smaller errors than small Δt_Ys. A closer look, however, reveals that strips of small errors pertain to odd Δt_Ys, and strips of larger errors to even Δt_Ys. This is an artefact of the applied autoregressive noise model, and can be illustrated by means of an example. Consider an autoregressive noise process of order 1 with autocorrelation structure:

$$\text{Cor}\{\tau\} = 0.5^{|\tau|} \tag{4.5}$$

Furthermore, suppose that a time series of observations Y of the process is available with even time steps Δt_Y=2. In order to model its spatial structure, the autocorrelation function of the observations is estimated and fitted by the following model:

$$\text{Cor}\{\tau\} = \phi^{|\tau|} \tag{4.6}$$

Since odd lag distances are missing, both ϕ=0.5 and ϕ=-0.5 describe the estimated autocorrelation function equally well (Fig. 4.5). If, however, Δt_Y represents an odd number, the presence of both odd and even lag distances prevents ϕ from becoming negative. A similar mechanism probably plays a role in Figs 4.3 and 4.4.

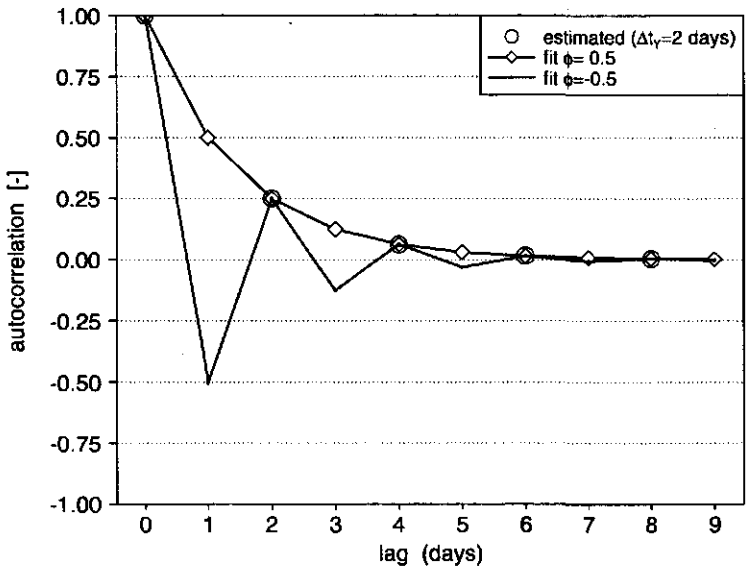

Fig. 4.5: Even lag distances result in two possible solutions of the calibration procedure. The fitted autocorrelations are connected by lines just to guide the eye.

The key-question now is, which method performs best, and under what conditions. This question can be answered by comparing the plots on the right in Figure 4.4 with those on the left. The difference in E{RMSE} between the methods provides a useful measure of relative performance, and is plotted in Fig. 4.6. Keep in mind that these plots only give a rough qualitative impression of the relative performances of the calibration methods. They are based on several assumptions, including educated guesses of the noise parameters themselves. Therefore, these plots should only be used as a rough guide line to obtain some insight in the relative performances.

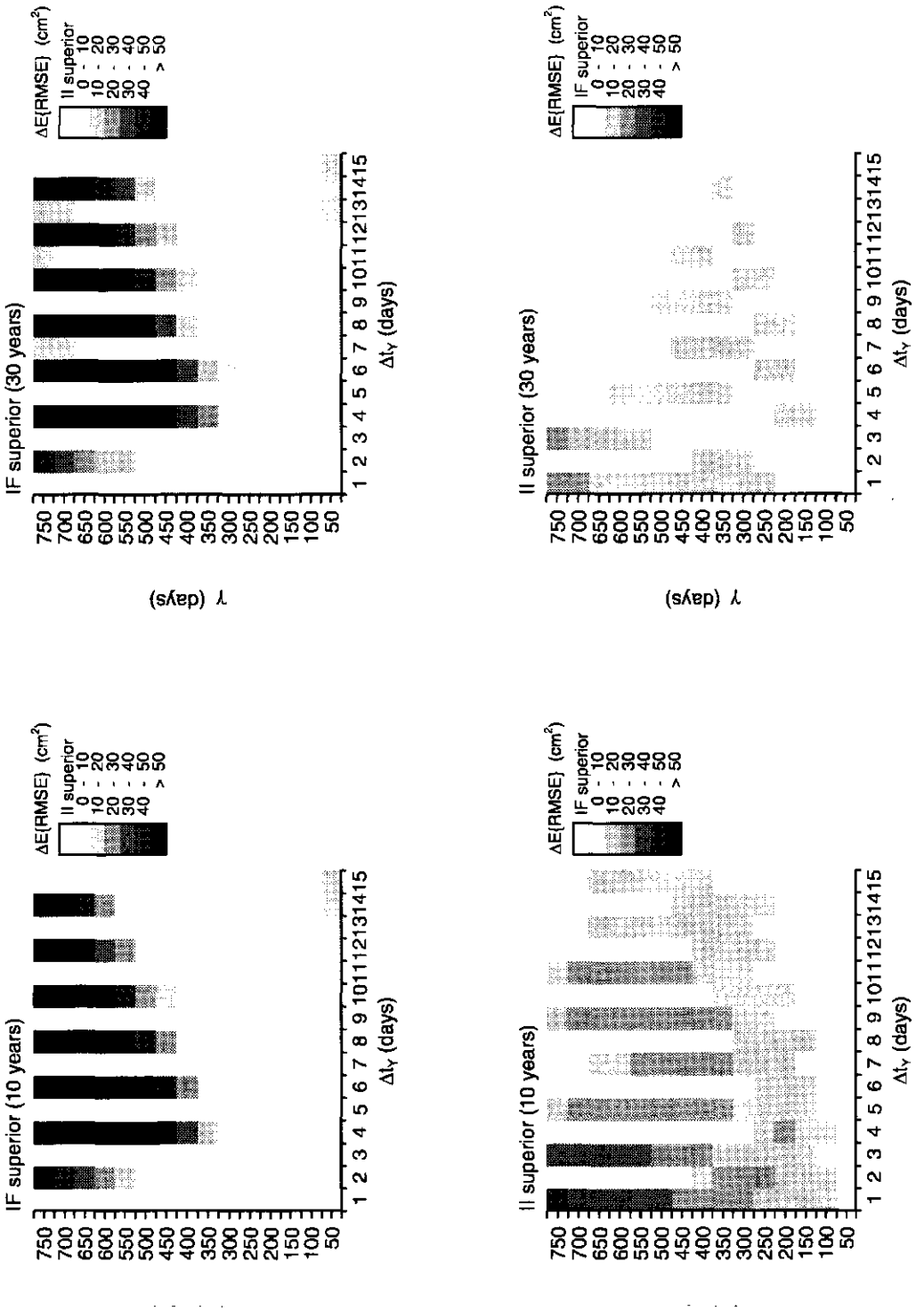

Fig. 4.6: Relative performances of the IF and II calibration methods, given the soil under study. The plots portray the areas in parameter space where IF is superior (top left: 10 years of data, and top right: 30 years of data), and where II is superior (bottom left: 10 years of data, and bottom right: 30 years of data).

5 Model application

In this chapter, EMERALD is confronted with real world data. After a brief description of the study area (section 5.1) and a summary of input data (section 5.2), the calibration of EMERALD is described (section 5.3). The calibrated model is verified, and its predictive power validated in section 5.4. In section 5.5 the ability of EMERALD to reproduce several univariate and bivariate statistics is tested. The chapter is concluded by giving some useful characteristics of groundwater dynamics based on simulation experiments (section 5.6).

5.1 Study area

EMERALD is applied to two observation wells in the vicinity of meteorological station Eelde, in the northeastern part of the Netherlands. The wells are coded 12EL0003 and 12BL0015. Groundwater depths are recorded twice a month, and stored in the On Line Groundwater Archive (OLGA) of NITG-TNO (Netherlands Institute for Applied Geosciences - Dutch Organisation for Applied Scientific Research). Knotters & Van Walsum (1995) give an elaborate description of the pedology and hydrology of the observations sites. A summary is given below:
Well 12EL0003 is located in a 100 cm thick peat soil on top of moderately fine sand (150-210 μm). Groundwater depths usually vary between 0-90 cm below the soil surface. Groundwater depths at well 12BL0015 are somewhat deeper, fluctuating between 20 and 150 cm below the soil surface. This well is situated in a loamy fine sandy soil. Both sites are covered with grass (pasture).

5.2 Model input

A summary of the model input is given in Table 5.1. Some entries need to be explained. First, the quotient of x and L is set to ½, which does not comply with the situation in the field. For reasons given in section 2.3.5 a value of ½ seemed more appropriate for both observation wells. Second the percolation zone has been discarded by setting f_b to unity. This seemed legitimate since the thicknesses of the percolation zones are small in both cases. Therefore, smoothing and delay play only a minor role, and are probably fully outweighed by the effects of bypass flow.

Table 5.1: Model input

characteristic	12BL0015	12EL0003	references
P and E_r	meteostation Eelde	meteostation Eelde	KNMI (1982-1991)
soil profile*)	0 - 55 cm B3	0 - 25 cm B16	Knotters & Van Walsum (1995)
	55 - 85 cm O3	25 - 100 cm O17	Wösten *et al.* (1994)
	85 - 180 cm O4	100 - 120 cm O2	
d_r	35 cm	20 cm	Stolp, personal communication
$f_{b,j} \quad \forall j$	1	1	-
f_c	1	1	Knotters & Van Walsum (1995)
$h_p(\theta_{fc})$	-100 cm	-100 cm	Knotters & Van Walsum (1995)
$h_{p,limiting}$	-500 cm	-500 cm	Knotters & Van Walsum (1995)
$h_{p,wilting}$	-8000 cm	-8000 cm	Knotters & Van Walsum (1995)
z_c	151 cm	120 cm	Wösten *et al.* (1994)
z_s	80 cm	30 cm	Knotters & Van Walsum (1995)
x/L	0.5	0.5	-
$\bar{d}_p$	35 cm	15 cm	-

*) codes refer to soil building blocks of the "Staringreeks" (Wösten *et al.*,1994)

5.3 Calibration

For both observation wells, a time series of observed groundwater depths, covering the period 1982-1991, was considered. The time series were split into a calibration and a validation period, each existing of five consecutive years. Hence, three periods were available for calibration, *i.e.* 1982-1986, 1987-1991, and 1982-1991. The deterministic component of EMERALD was calibrated by minimizing the objective function given in section 3.1. In order to estimate the internal noise parameters, the forward model approach was applied (section 3.2.2). The results are given in Tables 5.2 and 5.3.

Table 5.2: Calibrated parameters for observation well 12EL0003

period	γ (days)	μ (-)	q_v (mm/d)	ϕ (-)	σ_ε^2 (mm^2/d^2)
1982-1986	88	0.16	-2.32	0.79	0.0213
1987-1991	85	0.19	-3.23	-0.19	0.6207
1982-1991	86	0.17	-2.79	0.99	0.0002

Table 5.3: Calibrated parameters for observation well 12BL0015

calibration period	γ (days)	μ (-)	q_v (mm/d)	ϕ (-)	σ_ε^2 (mm^2/d^2)
1982-1986	305	0.29	-0.34	-0.98	0.5222
1987-1991	256	0.33	-0.40	-0.98	0.7448
1982-1991	274	0.31	-0.36	-0.98	0.6692

The calibrated parameter sets are very similar, except for q_v and the noise parameters of observation well 12EL0003. The first abberation is probably due to a trend in groundwater levels that can not be explained by the model. Therefore, q_v is assigned a lower value in the second period than in the first period. The dissimilarity in noise parameters is probably due to fast reaction times (small memory) of the groundwater system. This is reflected by relatively small drainage resistances. Therefore, observation density may be too sparse for accurate identification of the underlying autocovariance structure.

5.4 Verification and validation

Three measures were used to verify and validate the model, *i.e.* the mean error (ME), the root mean squared error (RMSE), and the fraction of significant errors (FSE). Error R is given by:

$$R(t_i) = Y(t_i) - h(t_i) \tag{5.1}$$

The mean error quantifies bias, and is defined as:

$$\mathrm{ME} = \frac{1}{n_Y} \sum_{i=1}^{n_Y} R(t_i) \tag{5.2}$$

The root mean squared error incorporates both bias and spread, and reads:

$$\mathrm{RMSE} = \sqrt{\frac{1}{n_Y} \sum_{i=1}^{n_Y} (R(t_i))^2} \tag{5.3}$$

Note that the objective function used to calibrate the deterministic component is equal to the mean squared error (MSE).

The third measure used in this study is the fraction of significant errors. This quantity is equal to the fraction of residuals outside the area bounded by the 2.5% and 97.5% percentiles:

$$FSE = \frac{1}{n_Y}\sum_{i=1}^{n_Y} I(R_i)$$

where: (5.4)

$$I(R_i) = \begin{cases} 0 & \text{if } |R_i| \le 2\sqrt{Var(H')} \\ 1 & \text{if } |R_i| > 2\sqrt{Var(H')} \end{cases}$$

Var{H'} is given by Eq.2.69. It is to be expected that five percent of the residuals R are outside the 2.5% en 97.5% percentile bounds, *i.e.* FSE=0.05. Recall that Eq.A4.11 is only an approximation is case of capillary rise. If more accurate bounds are required, the 2.5% and 97.5% percentiles should be obtained by simulation.

The following procedures were followed for verification and validation. First, on the basis of the parameter sets given in Tables 5.2 and 5.3, time series of $h(t_k)$ were predicted for the period 1982-1991. Next, the model was verified on the calibration periods and validated on the remaining periods by means of the measures given above. The results are presented in Tables 5.4 and 5.5.

The predictions are unbiased for the verification periods, and only slightly biased for the validation periods. Bias is due to the presence of trends not accounted for by the model. The accuracy of the predictions, as expressed by the RMSE, varies for both observation wells between 11.0 cm and 13.4 cm. Similar results for these wells were obtained by Knotters & Van Walsum (1995), Bierkens (1998a,b; 1999), and Bierkens & Walvoort (1998). The FSEs are generally somewhat too large. The same is true if the bounds were based on 1000 realizations instead of Eq.2.69 (Fig 5.1). For the 1982-1991 verification period, this results in FSEs of 0.11 and 0.08 for wells 12EL0003 and 12BL0015 respectively. Large FSEs are probably due to difficulties with the identification of the noise parameters.

Table 5.4: Verification and validation results for observation well 12EL0003. ME=mean error, RMSE=root mean squared error, FSE=fraction of significant errors.

calibration period	verification or validation period 1982-1986 ME (cm)	RMSE (cm)	FSE (-)	1987-1991 ME (cm)	RMSE (cm)	FSE (-)	1982-1991 ME (cm)	RMSE (cm)	FSE (-)
1982-1986	0.0	11.0	0.05	-7.3	13.4	0.08			
1987-1991	7.4	13.3	0.08	0.0	11.0	0.04			
1982-1991							0.0	11.7	0.11

Table 5.5: Verification and validation results for observation well 12BL0015. ME=mean error, RMSE=root mean squared error, FSE=fraction of significant errors.

calibration period	verification or validation period								
	1982-1986			1987-1991			1982-1991		
	ME (cm)	RMSE (cm)	FSE (-)	ME (cm)	RMSE (cm)	FSE (-)	ME (cm)	RMSE (cm)	FSE (-)
1982-1986	0.0	12.3	0.11	-3.8	12.6	0.10			
1987-1991	3.3	13.3	0.09	0.0	11.4	0.09			
1982-1991							0.0	12.1	0.08

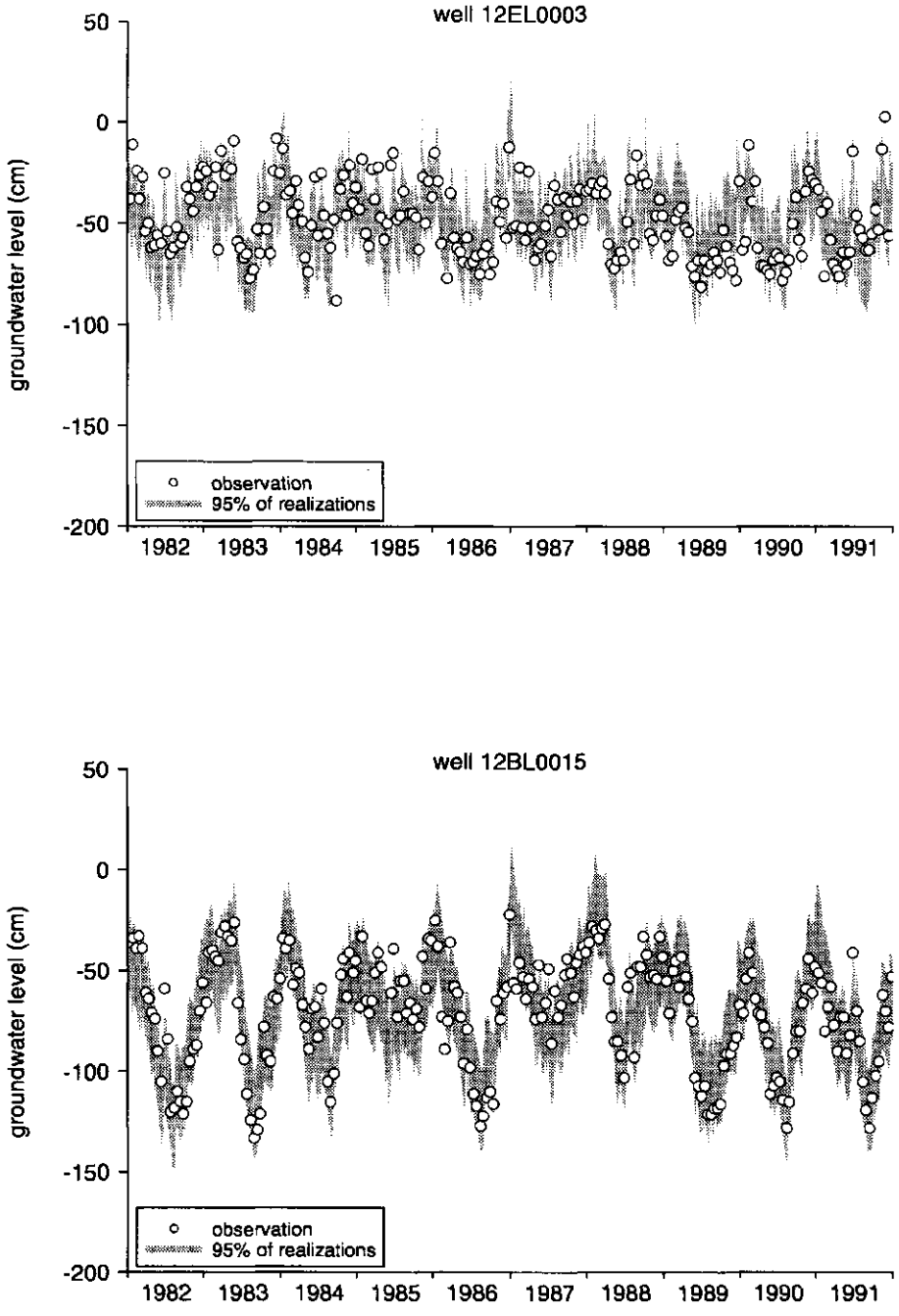

Fig. 5.1: Observed groundwater levels and the area where 95% of the realizations are in for 12EL0003 (top) and 12BL0015 (bottom). Calibration period: 1982-1991.

5.5 Reproducibility of univariate and bivariate statistics

In order to test if EMERALD correctly reproduces univariate statistics the following procedure was followed. First, 1000 time series were simulated for the calibration period 1982-1991. Next, univariate statistics were computed not for each realization separately, but for all realizations grouped together. These statistics were compared with those of observed time series. The results are visualised in Fig. 5.2 by means of box-whisker graphs. It can be concluded that EMERALD correctly reproduces univariate statistics.

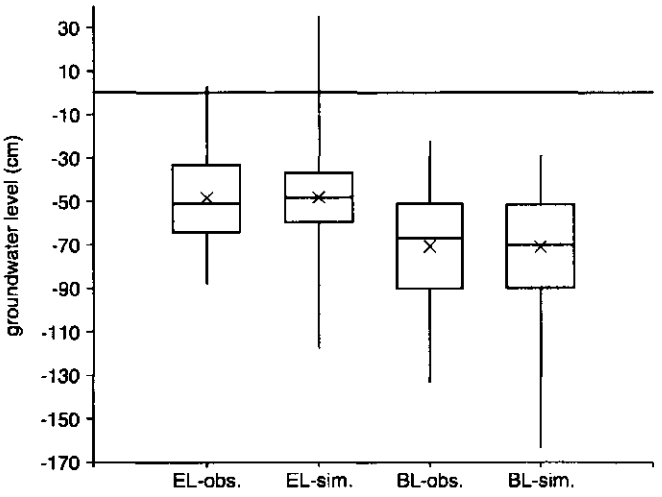

Fig. 5.2: Box-whisker diagrams for observed and simulated distributions. From left to right: well 12EL0003 observed and simulated, well 12BL0015 observed and simulated. The boxes represent the 25%, the 50% and the 75%-percentiles, the whiskers the minimum and the maximum values, and the crosses the arithmetic means.

Also the autocorrelation functions of observed and simulated groundwater levels were compared. The latter was obtained by averaging the 1000 autocorrelation functions of the realizations. The results are given in Figure 5.3. The autocorrelation functions pertaining to well 12EL0003 match very well. Those computed for well 12BL0015 are in phase, but differ somewhat in amplitude.

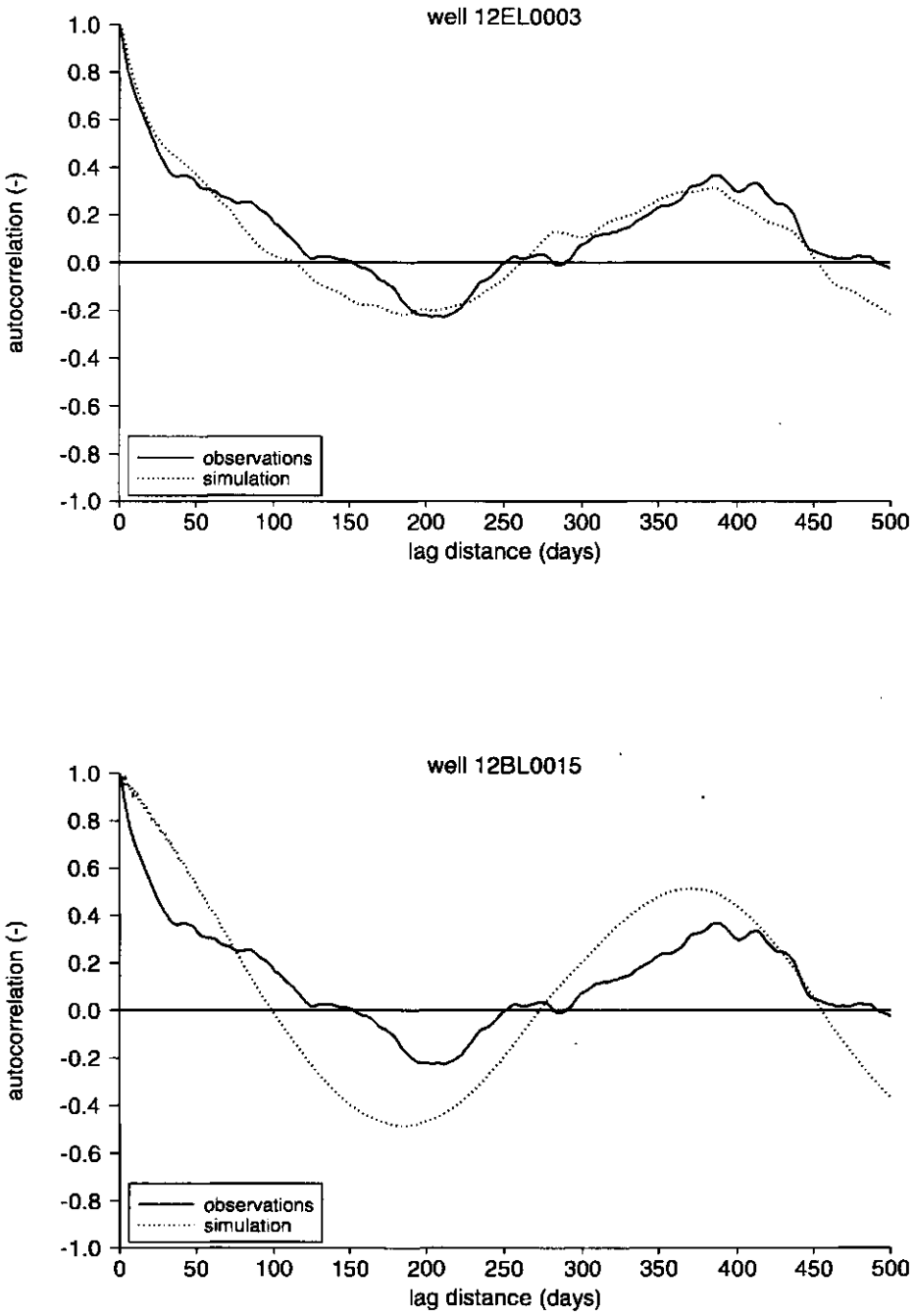

Fig. 5.3: Autocorrelation functions for well 12EL0003 (top) and well 12BL0015 (bottom) based on observations and simulation.

5.6 Derived measures of groundwater dynamics

Once a set of simulated time series of groundwater depths is available, numerous measures for describing groundwater dynamics can be derived. Some examples are the Mean Highest and Mean Lowest Water-table depths (MHW and MLW respectively), the frequency of exceedance graph (FOE-graph), and the regime curve. These measures will be addressed below.

The MLW and MHW are computed in two steps. First the three lowest and three highest groundwater depths during a year are determined and averaged. The resulting quantities are LG3 and HG3 respectively. The MLW is the arithmetical average of the LG3s during at least eight consecutive years. Similarly, the MHW is defined as the arithmetical average of the HG3s during this period. In order to compute these quantities, groundwater depths should be recorded twice a month. In Table 5.7 the MHWs and MLWs based on observations and simulation are given for the wells under study. These estimates pertain to the calibration period 1982-1991. It can be concluded that the MHWs and MLWs based on simulation closely resemble those based on observations.

Table 5.7: MHW and MLW based on observations and simulation. These characteristics pertain to the calibration period 1982-1991.

	12EL0003		12BL0015	
	observed	simulated	observed	simulated
MHW	-20.2	-24.2	-36.7	-33.2
MLW	-71.2	-71.9	-108.5	-107.1

A FOE-graph gives the probability that a specific groundwater level is exceeded. FOE-graphs for well 12EL0003 and well 12BL0015 are given in Figure 5.4. The solid curve is based on observations, the dashed one on 1000 realizations. As such, the latter represents both natural variation and model uncertainty. It can be concluded that the solid and dashed curves match very well.

The regime curves for the wells under study are plotted in Figure 5.5. A regime curve reflects the annual variation in groundwater levels. The shaded area in Figure 5.5 represents 95% of all realizations. As such, it resembles both natural variation and model uncertainty.

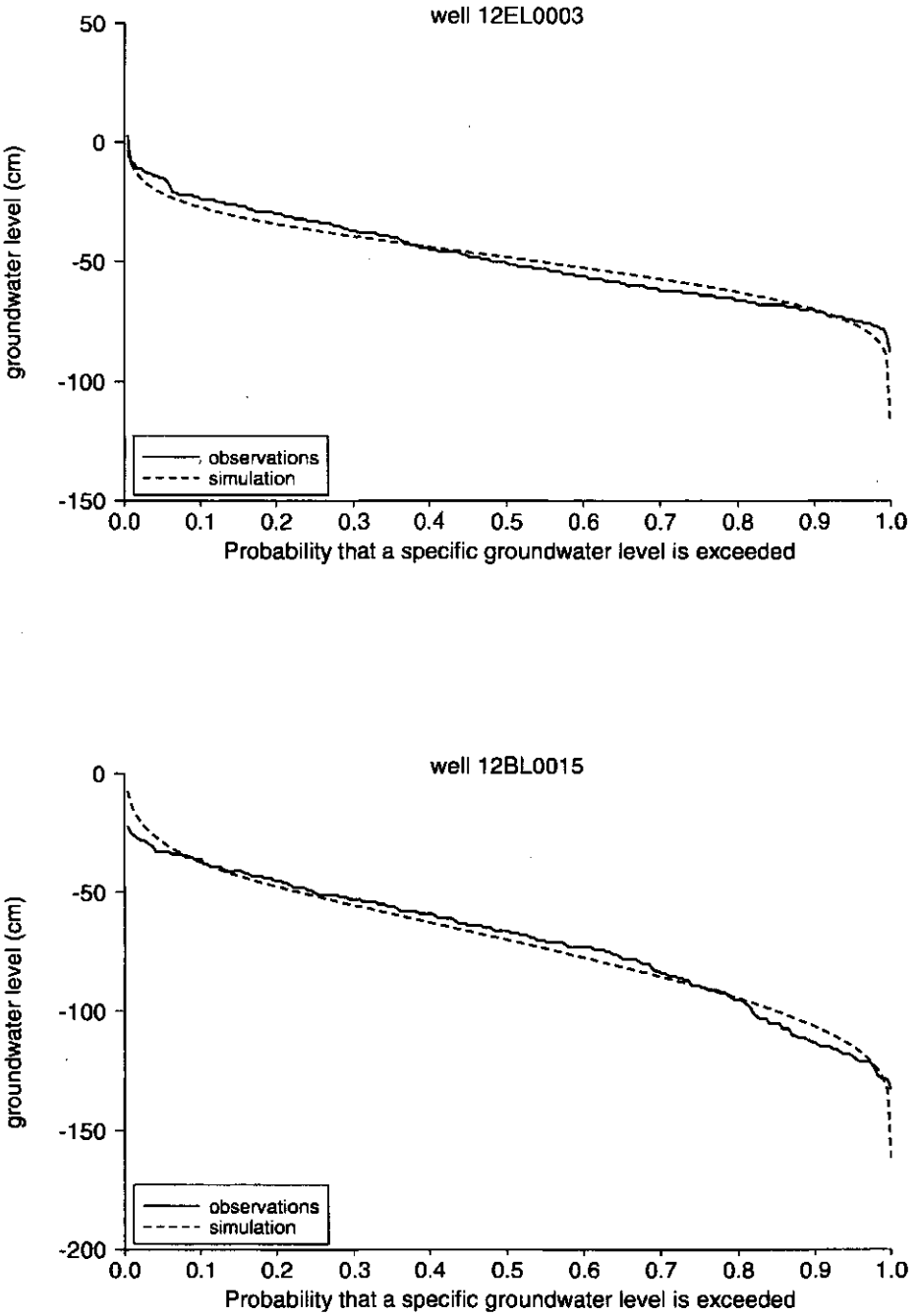

Fig. 5.4: Frequency of exceedance graphs based on observations and simulation for well 12EL0003 (top) and well 12BL0015 (bottom). The graphs represent the calibration period 1982-1991.

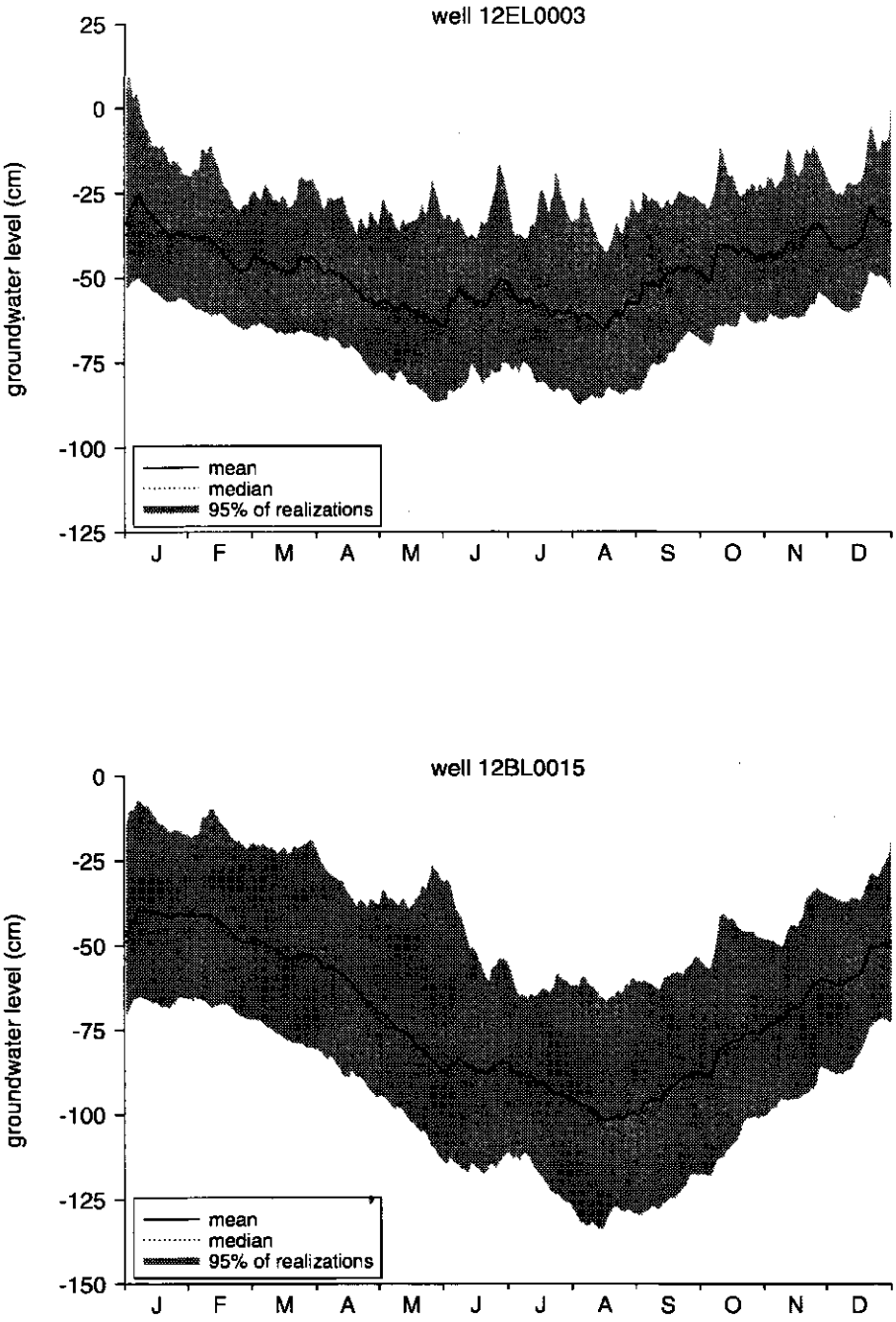

Fig. 5.5: Regime curves of well 12EL0003 (top) and well 12BL0015 (bottom). Both curves pertain to the calibration period 1982-1991.

6 Conclusions

EMERALD provides a means for rapid assessment of groundwater dynamics on a daily basis. It not only predicts important hydrological characteristics like groundwater depths and specific groundwater discharge, but it also quantifies the accuracy obtained. EMERALD describes three contiguous zones, *i.e.* the root zone, the percolation zone, and the groundwater zone. The root zone is modelled as a nonlinear reservoir. The model of the percolation zone is based on a linearized form of Richards' equation, while that of the groundwater zone is based on an analytical solution to the one-dimensional transient flow equation. Uncertainty is modelled by means of a first order autoregressive model.

A validation study revealed that EMERALD is able to make accurate predictions of various groundwater characteristics. Since calibration of its internal noise parameters can be troublesome, EMERALD is also equipped with an external noise model. EMERALD can be used to generate accurate time series of groundwater characteristics at sites where soil profile descriptions are available. A high resolution spatio-temporal description of the phreatic surface follows from interpolating these time series to a dense grid. This will be one of the challenging research topics for the future.

References

Bear, J., 1979. *Hydraulics of groundwater.* Israel, McGraw-Hill

Belmans, C. J.G. Wesseling & R.A. Feddes, 1983. *Simulation of the water balance of a cropped soil: SWATRE.* Journal of Hydrology 63: 271-286.

Bierkens, M.F.P., 1998a. *Eenvoudige stochastische modellen voor grondwaterstandsfluctuaties. Deel 1: Een stochastische differentiaalvergelijking.* Stromingen 4: 2, p.5-26.

Bierkens, M.F.P., 1998b. *Modeling water table fluctuations by means of a stochastic differential equation.* Water Resources Research 34: 2485-2499.

Bierkens, M.F.P., 1999. *Correction to "Modeling water table fluctuations by means of a stochastic differential equation, Water Resources Research 34: 2485-2499".* Water Resources Research 35: 1693.

Bierkens, M.F.P., & D.J.J. Walvoort, 1998. *Eenvoudige stochastische modellen voor grondwaterstandsfluctuaties. Deel 2: Gecombineerd bodem-grondwatermodel met stochastische invoer.* Stromingen 4: 3, p.5-18.

Box, G.E.P., G.M. Jenkins & G.C. Reinsel, 1994. *Time series analysis. Forecasting and control.* Third edition. New Jersey, Prentice Hall.

CHO (Commissie voor hydrologisch onderzoek TNO), 1986. *Verklarende hydrologische woordenlijst.* 's-Gravenhage, TNO, Rapporten en nota's No.16.

Dooge, J.C.I., 1973. *Linear theory of hydrologic systems.* United States Department of Agriculture, Technical Bulletin No. 1468.

Feddes, R.A., 1987. Crop factors in relation to Makkink reference-crop evapotranspiration. In: J.C. Hooghart, 1987. *Evaporation and weather.* CHO Proceedings and information No.39, p. 33-45.

Feddes, R.A., P.J. Kowalik, and H. Zaradny, 1978. *Simulation of field water use and crop yield.* Wageningen, Pudoc.

Gehrels, J.C., 1995. *Niet-stationaire grondwatermodellering van de Veluwe. Een studie naar de invloed van grondwaterwinning, inpoldering en verloofing op de grondwaterstand sinds 1951.* Amsterdam, Vrije Universiteit.

Knotters, M. & P.E.V. van Walsum, 1994. *Uitschakeling van weersinvloeden bij de karakterisering van het grondwaterstandsverloop.* Wageningen, DLO-Staring Centrum. Rapport 350.

Knotters, M. & P.E.V. van Walsum, 1997. *Estimating fluctuation quantities from time series of water-table depths using models with a stochastic component.* Journal of Hydrology 197: 25-46.

KNMI, 1982-1991. *MaandOverzicht van Neerslag en Verdamping in Nederland (MONV).* De Bilt, KNMI.

Koorevaar, P., G. Menelik, and C. Dirksen, 1983. *Elements of soil physics.* Amsterdam, Elsevier.

Kraijenhoff van de Leur, D.A., 1958. A study of non-steady groundwater flow with special reference to a reservoir-coefficient. *De Ingenieur* 70, 19: 87-94.

Wesseling, J.G., 1991. *Meerjarige simulatie van grondwaterstroming voor verschillende bodemprofielen, grondwatertrappen en gewassen met het model SWATRE.* Wageningen, DLO-Staring Centrum, Rapport 152.

Wiersum, L.K. & A. Reijmerink, 1990. *Beworteling.* Hoofdstuk 17 uit: Locher, W.P. & H. de Bakker, 1990. *Bodemkunde van Nederland. Deel 1: Algemene Bodemkunde.* Den Bosch, Malmberg.

Press, W.H., B.P. Flannery, S.A. Teukolsky, and W.T. Vetterling, 1989. *Numerical Recipes in Pascal. The Art of Scientific Computing.* Cambridge, Cambridge University Press.

Sluijs, P. van der, 1990. *Grondwatertrappen.* Hoofdstuk 11 uit: Locher, W.P. & H. de Bakker, 1990. *Bodemkunde van Nederland. Deel 1: Algemene Bodemkunde.* Den Bosch, Malmberg.

Wösten, J.H.M., G.J. Veerman & J. Stolte, 1994. *Waterretentie- en doorlatendheidskarakteristieken van boven- en ondergronden in Nederland: de Staringreeks.* Wageningen, DLO-Staring Centrum, Technisch Document 18.

De Zeeuw, J.W., 1966. *Analyse van het afvoerverloop van gebieden met hoofdzakelijk grondwaterafvoer. (Hydrograph analysis of areas with prevailing groundwater discharge).* Wageningen, PhD-thesis.

Zwamborn, M.H., 1995. *Modellering van de onverzadigde zone ten behoeve van grondwatermodellen.* Nieuwegein, Kiwa, SWI 95.142.

Annex 1 Linearization of Richards' equation

The derivation in this annex is largely based on Zwamborn (1995).
Richards' equation is given by:

$$\frac{\partial \theta}{\partial t} = \frac{\partial}{\partial z} k \left(\frac{\partial h_p}{\partial z} + 1 \right) \tag{A1.1}$$

where

θ = soil moisture content [-];
t = time [t];
k = hydraulic conductivity [Lt^{-1}];
h_p = pressure head of soil moisture [L];
z = vertical space coordinate [L].

In this expression, coordinate z is decreasing in downward direction. Both h_p and k are nonlinearly related to θ. A linear approximation of these variables can be obtained by means of Taylor expansion about θ_{eff}, *i.e.* the soil moisture content corresponding to the mean vertical flux in the percolation zone:

$$h_p(\theta) = \sum_{n=0}^{\infty} \frac{h_p^{(n)}(\theta_{eff})}{n!}(\theta-\theta_{eff})^n$$
$$= h_p(\theta_{eff}) + h_p'(\theta_{eff})(\theta-\theta_{eff}) + \frac{h_p''(\theta_{eff})}{2!}(\theta-\theta_{eff})^2 + \ldots \tag{A1.2}$$

$$k(\theta) = \sum_{n=0}^{\infty} \frac{k^{(n)}(\theta_{eff})}{n!}(\theta-\theta_{eff})^n$$
$$= k(\theta_{eff}) + k'(\theta_{eff})(\theta-\theta_{eff}) + \frac{k''(\theta_{eff})}{2!}(\theta-\theta_{eff})^2 + \ldots \tag{A1.3}$$

Neglecting all nonlinear terms gives:

$$h_p(\theta) \approx h_p(\theta_{eff}) + h_p'(\theta_{eff})(\theta-\theta_{eff}) \tag{A1.4}$$

$$k(\theta) \approx k(\theta_{eff}) + k'(\theta_{eff})(\theta-\theta_{eff}) \tag{A1.5}$$

Substituting Eqs A1.4 and A1.5 into Richards' equation, and neglecting all nonlinear terms yields:

$$\frac{\partial \theta}{\partial t} = k'(\theta_{eff})\frac{\partial \theta}{\partial z} + k(\theta_{eff})h_p'(\theta_{eff})\frac{\partial^2 \theta}{\partial z^2} \tag{A1.6}$$

In order to incorporate fluxes into this expression, it is first differentiated with respect to z and multiplied by $k(\theta_{eff})h_p'(\theta_{eff})$:

$$k(\theta_{eff})h_p'(\theta_{eff})\frac{\partial}{\partial z}\frac{\partial\theta}{\partial t} = k(\theta_{eff})h_p'(\theta_{eff})\frac{\partial}{\partial z}\left(k'(\theta_{eff})\frac{\partial\theta}{\partial z}\right)$$

$$+ k(\theta_{eff})h_p'(\theta_{eff})\frac{\partial}{\partial z}\left(k(\theta_{eff})h_p'(\theta_{eff})\frac{\partial^2\theta}{\partial z^2}\right) \qquad \text{(A1.7)}$$

$$\Leftrightarrow \frac{\partial}{\partial t}\left(k(\theta_{eff})h_p'(\theta_{eff})\frac{\partial\theta}{\partial z}\right) =$$

$$\frac{\partial}{\partial z}\left(k'(\theta_{eff})k(\theta_{eff})h_p'(\theta_{eff})\frac{\partial\theta}{\partial z}\right) + k(\theta_{eff})h_p'(\theta_{eff})\frac{\partial}{\partial z}\left[\frac{\partial}{\partial z}\left(k(\theta_{eff})h_p'(\theta_{eff})\frac{\partial\theta}{\partial z}\right)\right]$$

Next, the linear flux density equation is derived by substituting Eqs A1.4 and A1.5 into Darcy's law and neglecting all nonlinear terms:

$$q_z = -k(\theta)\left(\frac{\partial h_p(\theta)}{\partial z} + 1\right) \approx -k(\theta_{eff})h_p'(\theta_{eff})\frac{\partial\theta}{\partial z} - k(\theta_{eff}) \qquad \text{(A1.8)}$$

Rearranging gives:

$$k(\theta_{eff})h_p'(\theta_{eff})\frac{\partial\theta}{\partial z} = -q_z - k(\theta_{eff}) \qquad \text{(A1.9)}$$

This expression can be used to express θ in Eq.A1.7 in terms of q_z:

$$\frac{\partial(-q_z - k(\theta_{eff}))}{\partial t} = \frac{\partial}{\partial z}\left(k'(\theta_{eff})(-q_z - k(\theta_{eff}))\right) + k(\theta_{eff})h_p'(\theta_{eff})\frac{\partial}{\partial z}\left(\frac{\partial(-q_z - k(\theta_{eff}))}{\partial z}\right)$$

$$\Leftrightarrow \frac{\partial q_z}{\partial t} = k'(\theta_{eff})\frac{\partial q_z}{\partial z} + k(\theta_{eff})h_p'(\theta_{eff})\frac{\partial^2 q_z}{\partial z^2} \qquad \text{(A1.10)}$$

The resulting expression is the linear approximation of Richards' equation. It corresponds to the linear convection dispersion equation (*e.g.* Bear, 1979), where $k'(\theta_{eff})$ is the convection parameter, and $k(\theta_{eff})h_p'(\theta_{eff})$ the dispersion parameter.

Annex 2 The day-by-day method of De Zeeuw

In this annex, the convolutions of q_n and the pulse responses of q_d and h (Eq 2.49a and 2.47a) are rewritten according to the day-by-day method of the Zeeuw (1966).

First, Eq.2.46 is rewritten for discrete time steps $t_k=k\Delta t$ (k=0,1,...,∞):

$$U_{q_d}(k) = \frac{8}{\pi^2}\sum_{n=1,3,5}^{\infty} n^{-2}(\delta^{-n^2}-1)\,\delta^{kn^2} \tag{A2.1}$$

where $\delta = \exp\left(-\frac{\Delta t\pi^2}{8\mu\gamma}\right)$.

Next, Eq.A2.1 is split into a linear (first order) term, and a nonlinear term:

$$U_{q_d}(k) = \frac{8}{\pi^2}(\delta^{-1}-1)\delta^{k} + \frac{8}{\pi^2}\sum_{n=3,5,7}^{\infty} n^{-2}(\delta^{-n^2}-1)\delta^{kn^2} \tag{A2.2}$$

Let the nonlinear term be denoted by $\Delta U_{q_d}(k)$, then it follows:

$$\begin{aligned} U_{q_d}(k) &= \frac{8}{\pi^2}(\delta^{-1}-1)\delta^{k-1}\delta + \Delta U_{q_d}(k) \\ &= \frac{8}{\pi^2}(1-\delta)\delta^{k-1} + \Delta U_{q_d}(k) \end{aligned} \tag{A2.3}$$

If $q_d(t_0)$=0 then the specific groundwater discharge at time step t_1 equals:

$$\begin{aligned} q_d(t_1) &= q_n(t_1)U_{q_d}(1) \\ &= q_n(t_1)\left(\frac{8}{\pi^2}(1-\delta)\right) + q_n(t_1)\Delta U_{q_d}(1) \end{aligned} \tag{A2.4}$$

and at t_2:

$$\begin{aligned} q_d(t_2) &= q_n(t_1)U_{q_d}(2) + q_n(t_2)U_{q_d}(1) \\ &= q_n(t_1)\left(\frac{8}{\pi^2}(1-\delta)\right)\delta + q_n(t_1)\Delta U_{q_d}(2) \\ &+ q_n(t_2)\left(\frac{8}{\pi^2}(1-\delta)\right) + q_n(t_2)\Delta U_{q_d}(1) \end{aligned} \tag{A2.5}$$

Let

$$q_d^*(t_1) = q_n(t_1)\left[\frac{8}{\pi^2}(1-\delta)\right] \tag{A2.6}$$

and

$$q_d^{**}(t_1) = q_n(t_1)\Delta U_{q_d}(1) \tag{A2.7}$$

then

$$q_d(t_1) = q_d^*(t_1) + q_d^{**}(t_1) \tag{A2.8}$$

Similarly for t_2:

$$\begin{aligned} q_d^*(t_2) &= q_n(t_1)\left(\frac{8}{\pi^2}(1-\delta)\right)\delta + q_n(t_2)\left(\frac{8}{\pi^2}(1-\delta)\right) \\ &= q_d^*(t_1)\delta + q_n(t_2)\left(\frac{8}{\pi^2}(1-\delta)\right) \end{aligned} \tag{A2.9}$$

$$q_d(t_2) = q_d^*(t_2) + q_n(t_1)\Delta U_{q_d}(2) + q_n(t_2)\Delta U_{q_d}(1) \tag{A2.10}$$

In general, the specific groundwater discharge for time step t_k is given by:

$$q_d^*(t_k) = \delta q_d^*(t_{k-1}) + q_n(t_k)\left(\frac{8}{\pi^2}(1-\delta)\right) \tag{A2.11}$$

$$q_d(t_k) = q_d^*(t_k) + \sum_{i=1}^{k} q_n(t_{k-i+1})\Delta U_{q_d}(i) \tag{A2.12}$$

Thus far the day-by-day method. Computational efficiency can be further increased by neglecting terms of $\Delta U_{q_d}(i)$ for i=2,3,...,∞:

$$q_d^*(t_k) = \delta q_d^*(t_{k-1}) + q_n(t_k)\left(\frac{8}{\pi^2}(1-\delta)\right) \tag{A2.13}$$

$$q_d(t_k) = q_d^*(t_k) + q_n(t_k)\Delta U_{q_d}(1) \tag{A2.14}$$

Combining these state and output equations yields:

$$q_d(t_k) = \delta q_d(t_{k-1}) + \omega_0' q_n(t_k) + \omega_1' q_n(t_{k-1}) \tag{A2.15}$$

where

$$\delta = \exp\left(-\frac{\Delta t \pi^2}{8\mu\gamma}\right)$$

$$\omega_0' = \frac{8}{\pi^2}(1-\delta) + \Delta U_{q_a}(1)$$

$$\omega_1' = -\delta \Delta U_{q_a}(1)$$

$$\Delta U_{q_a}(1) = \frac{8}{\pi^2}\sum_{n=3,5,7}^{\infty} n^{-2}(1-\delta^{n^2})$$

The state and output equations with respect to h can be derived in a similar way, and read:

$$h^*(t_k) = \delta h^*(t_{k-1}) + q_n(t_k)\frac{32}{\pi^3}\gamma(1-\delta)\sin\left(\frac{\pi x}{L}\right) \quad \text{(A2.16)}$$

$$h(t_k) = h^*(t_k) + q_n(t_k)\Delta U_h(1) \quad \text{(A2.17)}$$

Combining Eqs A2.16 and A2.17 yields:

$$h(t_k) = \delta h(t_{k-1}) + \omega_0 q_n(t_k) + \omega_1 q_n(t_{k-1}) \quad \text{(A2.18)}$$

where

$$\delta = \exp\left(-\frac{\Delta t \pi^2}{8\mu\gamma}\right)$$

$$\omega_0 = \frac{32}{\pi^3}\gamma(1-\delta)\sin\left(\frac{\pi x}{L}\right) + \Delta U_h(1)$$

$$\omega_1 = -\delta \Delta U_h(1)$$

$$\Delta U_h(1) = \frac{32}{\pi^3}\gamma\sum_{n=3,5,7}^{\infty} n^{-3}(1-\delta^{n^2})\sin\left(\frac{n\pi x}{L}\right)$$

Annex 3 Autocovariance function of a temporally averaged AR(1)-process

Let $\bar{N}(t_k)$ denote the temporal mean of n time steps of the random process $N(t_k)$:

$$\bar{N}(t_k) = \frac{1}{n}\sum_{i=0}^{n-1} N(t_{k-i}) \tag{A3.1}$$

Furthermore, let each outcome of $N(t_k)$ be a realization of a zero-mean autoregressive process of order 1, with autocovariances (*e.g.* Chatfield, 1989):

$$\mathrm{Cov}\{N(t_k), N(t_{k+l})\} = \sigma_N^2 \phi^{|l|} = \frac{\sigma_\varepsilon^2}{1-\phi^2}\phi^{|l|} \tag{A3.2}$$

Then the autocovariance of $\bar{N}(t_k)$ is given by:

$$\begin{aligned}
\mathrm{Cov}\{\bar{N}(t_k), \bar{N}(t_{k+\tau})\} &= \mathrm{E}\left\{\left(\frac{1}{n}\sum_{i=0}^{n-1} N(t_{k-i})\right)\left(\frac{1}{n}\sum_{j=0}^{n-1} N(t_{k+\tau-j})\right)\right\} \\
&= \frac{1}{n^2}\sum_{i=0}^{n-1}\sum_{j=0}^{n-1} \mathrm{E}\{N(t_{k-i})N(t_{k+\tau-j})\} \\
&= \frac{1}{n^2}\sum_{i=0}^{n-1}\sum_{j=0}^{n-1} \mathrm{Cov}\{N(t_{k-i}), N(t_{k+\tau-j})\} \\
&= \frac{\sigma_\varepsilon^2}{(1-\phi^2)n^2}\sum_{i=0}^{n-1}\sum_{j=0}^{n-1} \phi^{|\tau+i-j|}
\end{aligned} \tag{A3.3}$$

In section 3.2.1, the sets of n random variables N are mutually exclusive. Therefore, τ should be a multiple of n, *i.e.* $\tau \in \{0,n,2n,3n,...,\infty\}$.

For $\tau \geq n$ the double summation in Eq.A3.3 can be eliminated. First Eq.A3.3 is written as:

$$Cov\{\bar{N}(t_k), \bar{N}(t_{k+\tau})\} = \begin{cases} \dfrac{\sigma_\varepsilon^2}{(1-\phi^2)n^2}\displaystyle\sum_{i=0}^{n-1}\sum_{j=0}^{n-1} \phi^{\tau+i-j} & \text{if } j-i \leq \tau \\ \dfrac{\sigma_\varepsilon^2}{(1-\phi^2)n^2}\displaystyle\sum_{i=0}^{n-1}\sum_{j=0}^{n-1} \phi^{-\tau+j-i} & \text{if } j-i > \tau \end{cases} \tag{A3.4}$$

Since j-i is always smaller than or equal to τ for $\tau \geq n$, Eq.A3.4 can be written as:

$$Cov\{\bar{N}(t_k), \bar{N}(t_{k+\tau})\} = \frac{\sigma_\varepsilon^2}{(1-\phi^2)n^2} \sum_{i=0}^{n-1} \sum_{j=0}^{n-1} \phi^{\tau+i-j} \qquad \text{for } \tau \geq n \tag{A3.5}$$

Elimination of the finite geometric sequences in this expression finally yields:

$$\begin{aligned}
Cov\{\bar{N}(t_k), \bar{N}(t_{k+\tau})\} &= \frac{\sigma_\varepsilon^2}{(1-\phi^2)n^2} \sum_{i=0}^{n-1} \sum_{j=0}^{n-1} \phi^{\tau+i-j} \\
&= \frac{\sigma_\varepsilon^2}{(1-\phi^2)n^2} \phi^{\tau} \sum_{i=0}^{n-1} \phi^{i} \sum_{j=0}^{n-1} \phi^{-j} \\
&= \frac{\sigma_\varepsilon^2}{(1-\phi^2)n^2} \phi^{\tau} \left(\frac{1-\phi^n}{1-\phi}\right)\left(\frac{1-\phi^{-n}}{1-\phi^{-1}}\right) \\
&= \frac{\sigma_\varepsilon^2}{(1-\phi^2)n^2} \phi^{\tau-n} \left(\frac{1-\phi^n}{1-\phi}\right)\left(\frac{\phi^n-1}{1-\phi^{-1}}\right) \\
&= \frac{\sigma_\varepsilon^2}{(1-\phi^2)n^2} \phi^{\tau-n} \left(\frac{1-\phi^n}{1-\phi}\right)\left(\frac{\phi(\phi^n-1)}{\phi-1}\right) \\
&= \frac{\sigma_\varepsilon^2}{(1-\phi^2)n^2} \phi^{\tau-n} \left(\frac{1-\phi^n}{1-\phi}\right)\left(\frac{\phi(1-\phi^n)}{1-\phi}\right) \\
&= \frac{\sigma_\varepsilon^2}{(1-\phi^2)n^2} \phi^{\tau-n+1} \left(\frac{1-\phi^n}{1-\phi}\right)^2 \qquad \text{for } \tau \in \{n, 2n, 3n, ..., \infty\}
\end{aligned} \tag{A3.6}$$

In short, Eq. A3.3 should be used for $\tau=0$, and Eq.A3.6 for $\tau \in \{n, 2n, 3n, ..., \infty\}$.

Annex 4 Autocovariance functions of prediction errors of groundwater levels and specific discharge

The prediction error of H is defined as the difference between its true value and its prediction:

$$H_k' = H_k - \mathrm{E}\{H_k\} \tag{A4.1}$$

where $H_k = H(t_k)$. Note that the true value has been modelled as the outcome of a random variable.

The autocovariance of points separated by lag τ is given by:

$$\mathrm{Cov}\{H_k', H_{k+\tau}'\} = \mathrm{E}\{H_k' H_{k+\tau}'\} - \mathrm{E}\{H_k'\}\mathrm{E}\{H_{k+\tau}'\} \tag{A4.2}$$

Since $\mathrm{E}\{H_k'\}=0 \quad \forall k$, Eq.A4.2 is identical to:

$$\mathrm{Cov}\{H_k', H_{k+\tau}'\} = E\{H_k' H_{k+\tau}'\} \tag{A4.3}$$

In order to facilitate the derivation of the autocovariance function of H', Q_n is assumed to be independent of H, and therefore deterministic, *i.e.* $Q_n\{H_k\}\equiv q_n$, and $q_n' = q_n - \mathrm{E}\{q_n\} = 0$. Consequently, Eq.2.55 can be written as:

$$H_k' = \delta H_{k-1}' + \omega_0 N_k' + \omega_1 N_{k-1}' \tag{A4.4}$$

Expanding this expression gives:

$$\begin{aligned} H_k' &= \delta H_{k-1}' + \omega_0 N_k' + \omega_1 N_{k-1}' \\ &= \delta^2 H_{k-2}' + \delta\omega_0 N_{k-1}' + \delta\omega_1 N_{k-2}' + \omega_0 N_k' + \omega_1 N_{k-1}' \\ &= \ldots \\ &= \sum_{i=0}^{\infty} \delta^i(\omega_0 N_{k-i}' + \omega_1 N_{k-i-1}') \end{aligned} \tag{A4.5}$$

and

$$H_{k+\tau}' = \sum_{i=0}^{\infty} \delta^i(\omega_0 N_{k+\tau-i}' + \omega_1 N_{k+\tau-i-1}') \tag{A4.6}$$

Substituting Eqs A4.5 and A4.6 into Eq.A4.3 gives:

$$\begin{aligned}
\mathrm{Cov}\{H_k', H_{k+\tau}'\} = \mathrm{E}\{&(\sum_{i=0}^{\infty} \delta^i \omega_0 N_{k-i}' + \sum_{i=0}^{\infty} \delta^i \omega_1 N_{k-i-1}') \\
&\cdot(\sum_{j=0}^{\infty} \delta^j \omega_0 N_{k+\tau-j}' + \sum_{j=0}^{\infty} \delta^j \omega_1 N_{k+\tau-j-1}')\} \\
&= \omega_0^2 \sum_{i=0}^{\infty}\sum_{j=0}^{\infty} \delta^{i+j} \mathrm{E}\{N_{k-i}' N_{k+\tau-j}'\} \\
&+ \omega_0\omega_1 \sum_{i=0}^{\infty}\sum_{j=0}^{\infty} \delta^{i+j} \mathrm{E}\{N_{k-i-1}' N_{k+\tau-j}'\} \\
&+ \omega_0\omega_1 \sum_{i=0}^{\infty}\sum_{j=0}^{\infty} \delta^{i+j} \mathrm{E}\{N_{k-i}' N_{k+\tau-j-1}'\} \\
&+ \omega_1^2 \sum_{i=0}^{\infty}\sum_{j=0}^{\infty} \delta^{i+j} \mathrm{E}\{N_{k-i-1}' N_{k+\tau-j-1}'\}
\end{aligned} \tag{A4.7}$$

Recall that the lag τ-autocovariance of AR(1)-process N is given by:

$$E\{N_k' N_{k+\tau}'\} = \phi^{|\tau|} \sigma_N^2 = \phi^{|\tau|} \frac{\sigma_\varepsilon^2}{1-\phi^2} \tag{A4.8}$$

Substituting this expression into Eq.A4.7 gives:

$$\begin{aligned}
\mathrm{Cov}\{H_k', H_{k+\tau}'\} = &\frac{\sigma_\varepsilon^2}{1-\phi^2} \omega_0^2 \sum_{i=0}^{\infty}\sum_{j=0}^{\infty} \delta^{i+j} \phi^{|\tau+i-j|} + \frac{\sigma_\varepsilon^2}{1-\phi^2} \omega_0\omega_1 \sum_{i=0}^{\infty}\sum_{j=0}^{\infty} \delta^{i+j} \phi^{|\tau+i-j+1|} \\
&+ \frac{\sigma_\varepsilon^2}{1-\phi^2} \omega_0\omega_1 \sum_{i=0}^{\infty}\sum_{j=0}^{\infty} \delta^{i+j} \phi^{|\tau+i-j-1|} + \frac{\sigma_\varepsilon^2}{1-\phi^2} \omega_1^2 \sum_{i=0}^{\infty}\sum_{j=0}^{\infty} \delta^{i+j} \phi^{|\tau+i-j|} \\
= &\frac{\sigma_\varepsilon^2}{1-\phi^2} \Bigg[(\omega_0^2+\omega_1^2) \sum_{i=0}^{\infty}\sum_{j=0}^{\infty} \delta^{i+j} \phi^{|\tau+i-j|} \\
&+ \omega_0\omega_1 \left(\sum_{i=0}^{\infty}\sum_{j=0}^{\infty} \delta^{i+j} \phi^{|\tau+i-j+1|} + \sum_{i=0}^{\infty}\sum_{j=0}^{\infty} \delta^{i+j} \phi^{|\tau+i-j-1|} \right) \Bigg]
\end{aligned} \tag{A4.9}$$

Evaluation of the infinite geometric sequences finally gives:

$$\mathrm{Cov}\{H_k', H_{k+\tau}'\} =$$

$$= \sigma_\varepsilon^2 \frac{(\omega_0^2+\omega_1^2)(\delta^{-\tau}+\phi\delta^{\tau+1}+\eta_1)+\omega_0\omega_1[\delta^{1-\tau}+\delta^{-1-\tau}+\phi\delta^{\tau}(1+\delta^2)+\eta_2+\eta_3]}{(1-\phi^2)(1-\delta\phi)(1-\delta^2)} \qquad \text{(A4.10)}$$

where

$$\eta_1 = \begin{cases} 0 & \text{for } \tau = 0 \\ \dfrac{1-\phi\delta}{1-\phi/\delta}\left(\delta^{\tau}-\phi^{\tau}\right)-\delta^{-\tau}+\phi^{\tau} & \text{for } \tau=1,2,\ldots,\infty \end{cases}$$

$$\eta_2 = \begin{cases} 0 & \text{for } \tau\in\{0,1\} \\ \dfrac{1-\phi\delta}{1-\phi/\delta}\left(\delta^{\tau-1}-\phi^{\tau-1}\right)-\delta^{1-\tau}+\phi^{\tau-1} & \text{for } \tau=2,3,\ldots,\infty \end{cases}$$

$$\eta_3 = \frac{1-\phi\delta}{1-\phi/\delta}\left(\delta^{\tau+1}-\phi^{\tau+1}\right)-\delta^{-\tau-1}+\phi^{\tau+1} \qquad \text{for } \tau=0,1,\ldots,\infty$$

Applying this expression for $\tau=0$ gives the variance of H_k':

$$\mathrm{Var}\{H_k'\} = \sigma_\varepsilon^2 \frac{(\omega_0^2+\omega_1^2)(1+\delta\phi)+2\omega_0\omega_1(\delta+\phi)}{(1-\phi^2)(1-\delta\phi)(1-\delta^2)} \qquad \text{(A4.11)}$$

The autocovariance of Q_d' can be derived analogously to that of H'. The resulting expression is very similar to Eq.A4.10, except that the moving average parameters ω_0 and ω_1 should be replaced by ω_0' and ω_1' respectively.

Annex 5 User's manual EMERALD (version: July 1998)

Introduction

EMERALD is implemented on a personal computer. It is written in Borland's Turbo Pascal (version 7.0) for MS-DOS. A data flow diagram (DFD) of EMERALD is given in Figure A5.1. In this diagram, processes are denoted by circles, temporary files by two parallel horizontal lines, user accessible files by boxes, and data flows by arrows.

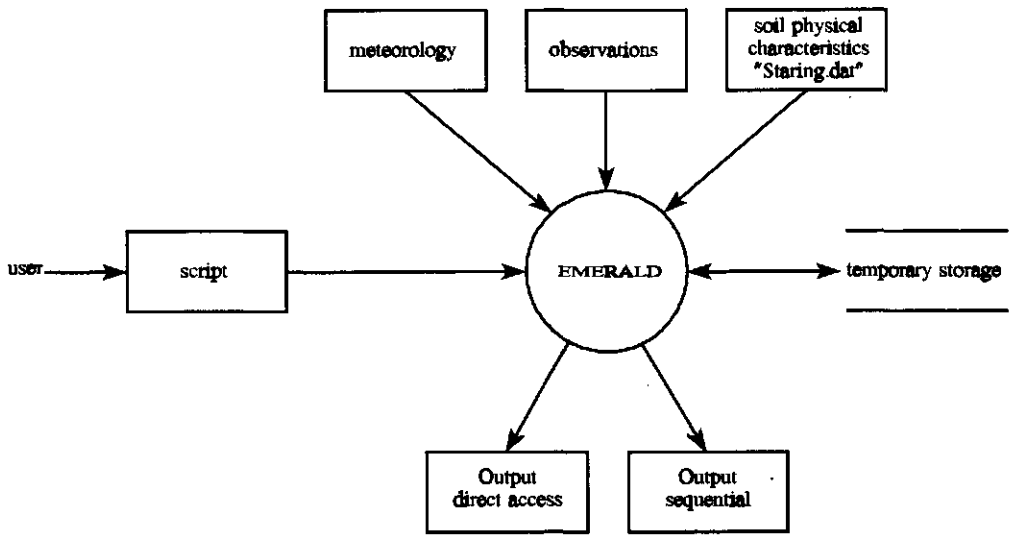

Fig. A5.1: Data flow diagram of EMERALD

EMERALD is driven by a script file, which takes a central position in the DFD. A script file contains a high-level computer language, *i.e.* the script, which prescribes which actions to perform, which files to read, and where to store results. At run-time, EMERALD reads the script, deciphers it by means of its built-in script interpreter, and carries out the appointed tasks. Each line in the script file consists of a script directive and associated parameters. In general, the syntax reads:

DIRECTIVE <mandatory_parameter> [optional_parameter] <option_1 | option_2>

Throughout this manual, mandatory parameters are given in angular brackets and optional parameters in square brackets. Furthermore, piping symbols, *i.e.* |, are used to separate two or more options. Only one of these options should be selected. Annotations should be preceded by a "+" on the first position of each commentary line in the script file. Parameters printed in italics and greek symbols should be replaced by appropriate numeric values, parameters printed upright should simply be copied. EMERALD's script language is order invariant. This means that the user can put the script directives in any order (s)he prefers. However, if EMERALD encounters a directive more than once, only the first is processed.

Script directives

In this section the script directives are addressed in alphabetical order.

BINARY	*output*
syntax:	BINARY <* | [Ea] [Ep] [V] [qp] [qg] [qc] [qn] [h] [qd]>
purpose:	Stores output in direct access files. In case of simulation, storage of all realizations may take up a substantial amount of disk space. In order to suppress this demand, EMERALD offers the opportunity to store the realizations in direct access format. This can be effectuated by means of the BINARY-directive. Its syntax is very similar to the OUTPUT-directive, except that no output file name(s) can be specified. EMERALD uses default file names which consist of the parameter name of interest plus extension *rl4*, *e.g. Ea.rl4*, *Ep.rl4*, and *V.rl4*. A description of these binary files is given in a subsequent section.
example:	BINARY h qd

BYPASS	*model parameters*
syntax:	BYPASS <$f_{b,1}$> [$f_{b,2}$] ... [$f_{b,9}$]
purpose:	Governs the amount of bypass flow through subsoil layers 1 to 9. $f_{b,j}$ should be expressed as a fraction of the incoming flux of subsoil layer j.
example:	BYPASS 0.5 0.2 0.1

CALIBRATION	*action*
syntax:	CALIBRATION < [D] [II] [IF] [EF] > [tolerance]
purpose:	Specifies the calibration method(s) to perform. The deterministic component is calibrated when D is encountered on the parameter line, the stochastic component is calibrated when II, IF, and/or EF are encountered. These abbreviations stand for Internal noise - Inverse model, Internal noise - Forward model, and External noise - Forward model respectively. Optionally, the tolerance of the termination criterium of the Downhill-Simplex method may be specified (Press *et al.*, 1989). When II, IF, and/or EF are supplied as parameters, EMERALD expects the observations in the observation file to be separated by approximately equal time steps (section 3.2). Furthermore, if II is specified, EMERALD replaces missing values by predictions obtained by linear interpolation.
example:	CALIBRATION D IF EF 1e-6

CROP *model parameters*

syntax: CROP <f_c> <$h_{p,fc}$> <$h_{p,lp}$> <$h_{p,wp}$> <*|z_c>

purpose: Supplies EMERALD with crop and soil specific parameters. The parameter line should contain the following quantities:

f_c = crop factor [-];
$h_{p,fc}$ = pressure head at field capacity (cm);
$h_{p,lp}$ = pressure head at limiting point (cm);
$h_{p,wp}$ = pressure head at wilting point (cm);
z_c = critical depth (cm);
* = critical depth according to Wösten *et al.*, (1994) (cm).

EMERALD makes no distinction between positive and negative pressure heads.

example: CROP 1 -100 -500 -8000 *

DRAINAGE *model parameters*

syntax: DRAINAGE <z_d> <x> <L>

purpose: Specifies the drainage parameters:

z_d= level of drainage base with respect to soil surface (cm);
x= lateral space coordinate (see Figure 2.1) [L];
L= distance between drainage courses (see Figure 2.1) [L].

See to it that x and L have corresponding units.

example: DRAINAGE -100 50 100

FIX *action*

syntax: FIX <[gamma] [mu] [qv] [phi] [sigma2]>

purpose: Keeps the parameters on the parameter line fixed to their initial values during calibration. The initial values should be specified by the GROUNDWATER and NOISE directives.

example: FIX gamma phi

GROUNDWATER *model parameters*

syntax: GROUNDWATER <μ> <γ> <q_v> <*|h_{avg}> <$q_{g,avg}$>

purpose: Provides the parameters of the saturated zone. The parameter line should contain the following quantities:

μ = specific yield [-];
γ = drainage resistance (days);
q_v = infiltration/seepage flux (mm/d);
h_{avg} = average groundwater level (cm);
* = average groundwater level is based on observation file (cm);
$q_{g,avg}$ = average flux in percolation zone (mm/y).

Groundwater levels should be given with respect to the soil surface.

example: GROUNDWATER 0.2 200 0 * 250

INITIAL *model parameters*

syntax: INITIAL <S_0> <*|h_0> <q_{d0}> <q_{n0}> <N_0>

purpose: Gives the initial values of the following parameters:

S_0	= initial saturation grade root zone [-];
h_0	= initial groundwater level with respect to the soil surface (cm);
*	= h_0 equals the average groundwater level in the observation file (cm);
q_{d0}	= initial specific discharge (mm/d);
q_{n0}	= initial net input to the groundwater system (mm/d);
N_0	= initial value of noise process N.

The following default values are used if this directive is omitted: S_0 ~ field capacity, h_0 ~ drainage base, q_{d0}, q_{n0}, and N_0 are set to zero.

example: INITIAL 0.8 * 0 0 0

LAGS *action*

syntax: LAGS <n_{fit}> [n_{print}]

purpose: Specifies the number of lags involved in fitting the autocovariance function (section 3.2). The optional parameter n_{print} specifies the number of lags that should be written to the output file. n_{print} should always be greater than or equal to n_{fit}. If the LAGS - directive is omitted, n_{fit} and n_{print} are set to 10 by default, *i.e.* lags 0 to 9 are used for fitting.

example: LAGS 15 20

METEO *input*

syntax: METEO <*file_name*> [*skip*]

purpose: Specifies the name of the file containing time series of precipitation amounts and evapotranspiration. Its file format is given in a subsequent section. The optional parameter [*skip*] denotes the number of lines to skip in the meteo file (default: *skip*=0).

example: METEO Eelde.met 1

NOISE *model parameters*

syntax: NOISE <ϕ> <σ_ε^2>

NOISE <ϕ> <σ_ε^2> <INTERNAL | EXTERNAL>

purpose: Specifies the parameters of the noise process. The first is sufficient to supply the initial values in case of calibration, the latter is required in case of simulation. In case of prediction, the variance of the prediction errors of h and/or q_d are given if the noise type is set to INTERNAL.

example: NOISE 0.25 0.01 INTERNAL

OBSERVATIONS	*input*
syntax:	OBSERVATIONS *<day1> <year1> <day2> <year2> <file_name> [skip]*
purpose:	Specifies which part of observation file *<file_name>* should be processed. The period of interest starts at *<day1>* of *<year1>* and ends at *<day2>* of *<year2>*. *[skip]* refers to the number of lines to skip in *<file_name>*, and is 0 by default.
example:	OBSERVATIONS 1 1982 365 1991 12BL0015.dat 1

OUTPUT	*output*
syntax:	OUTPUT *<file_name>* OUTPUT *<file_name>* <* | [P] [Ea] [Er] [Ep] [V] [qp] [qg] [qc] [qn] [h] [qd]>
purpose:	Creates output file *<file_name>* which gives a summary of input parameters, and a detailed description of model output. In case of prediction or simulation, the requested output should be enumerated after *<file_name>*. The mnemonics on the parameter line correspond to those used in the report. If the symbol * is used, all parameters on the parameter line are written to *<file_name>*. In case of calibration, it is sufficient to supply *<file_name>*.
example:	OUTPUT Emerald.out h qd

PREDICTION	*action*
syntax:	PREDICTION *<day1> <year1> <day2> <year2>*
purpose:	Performs prediction. The parameter line specifies the start and end of the prediction period, *i.e.* *<day1>* of *<year1>* and *<day2>* of *<year2>* respectively. If the script contains the OBSERVATION-directive, validation and/or verification measures are computed for the time span that is part of both the prediction period and the observation period.
example:	PREDICTION 1 1982 365 1991

PRERUN	*action*
syntax:	PRERUN <* | *#years>*
purpose:	Specifies the length of the prerun or warming up period. A prerun of *<#years>* years is required to eliminate the effect of the initial values. The prerun period starts at the first day in the meteo file if <*> is encountered on the parameter line.
example:	PRERUN 2.5

SIMULATION	*action*
syntax:	SIMULATION *<day1> <year1> <day2> <year2> <#runs> <#runs_out> <seed>*
purpose:	Performs simulation. The parameter line specifies the start and end of the simulation period, *i.e.* *<day1>* of *<year1>* and *<day2>* of *<year2>* respectively, the number of realizations to perform *<#runs>*, the number of realizations to write to the output file *<#runs_out>*, and the random seed *<seed>* to initiate the pseudo random number generator (*gasdev/ran1* of Press *et al.* (1989)).
example:	SIMULATION 1 1982 365 1991 1000 1 12534

SOIL	*model parameters*
syntax:	SOIL *<topsoil=thickness> <subsoil1=thickness> ... [subsoil9=thickness] [cut_off]*
purpose:	Specifies the soil physical characteristics of the unsaturated zone. The parameter line contains building blocks of the *Staringreeks* (Wösten *et al.*, 1994), together with their associated thicknesses (cm). A total of nine subsoil layers may be specified. The root zone is represented by the topsoil layer, the percolation zone by the subsoil layers. The amount of percolation not reaching the groundwater system due to truncation of the pulse response function $U_p(\Delta t,t)$ is governed by *[cut_off]*. This quantity should be expressed as a fraction of the total amount of percolation. It significantly affects the amount of CPU-time required. Default value: 1E-6.
example:	SOIL B3=30 B3=20 O3=100 1e-5

TMPDIR	*general*
syntax:	TMPDIR *<path>*
purpose:	Designates the path to temporary files. Model performance may be significantly improved if *<path>* denotes a RAM-drive.
example:	TMPDIR e:\tmp

Examples of script files

In Figures A5.1 and A5.2 examples of script files are given. These scripts were also used for the case study of Chapter 5.

```
+ + + + + + + + + + + + + + + + + + + + + + + + + + + + + + + + + +
+                                                                 +
+  Calibration of the deterministic and stochastic                +
+  components (internal noise, forward model),                    +
+  followed by prediction (verification)                          +
+                                                                 +
+  period   : 1982-1986                                           +
+  well     : 12BL0015                                            +
+  location : Vries, Eelde                                        +
+                                                                 +
+ + + + + + + + + + + + + + + + + + + + + + + + + + + + + + + + + +

CALIBRATION D IF 1e-9
LAGS 20 20
PREDICTION 1 1982 365 1986
OBSERVATIONS 1 1982 365 1986 12BL0015.dat 5
METEO Eelde.met 1
PRERUN 2
OUTPUT prediction.out h
CROP 1 100 500 8000 *
SOIL B3=35 B3=20 O3=30 O4=95 1e-6
GROUNDWATER 0.2 165 0 * 261
DRAINAGE  80 1 2
INITIAL 1 * 0 0 0
BYPASS 1 1 1
NOISE 0 0.001 INTERNAL
```

Fig. A5.2: verification script

```
+ + + + + + + + + + + + + + + + + + + + + + + + + + + + + + + + + + + + + +
+                                                                         +
+ Calibration of the deterministic and stochastic                         +
+ components (internal noise, forward model),                            +
+ followed by simulation.                                                 +
+                                                                         +
+ period   : 1982-1991                                                   +
+ well     : 12BL0015                                                    +
+ location : Vries, Eelde                                                +
+                                                                         +
+ + + + + + + + + + + + + + + + + + + + + + + + + + + + + + + + + + + + + +

CALIBRATION D IF 1e-9
LAGS 20 20
SIMULATION   1 1982 365 1991 1000 2 12534
OBSERVATIONS 1 1982 365 1991 12BL0015.dat 5
METEO Eelde.met 1
PRERUN 2
OUTPUT Simulation.out h qd
BINARY h qd
CROP 1 100 500 8000 *
SOIL B3=35 B3=20 O3=30 O4=95 1e-6
GROUNDWATER 0.2 165 0 * 261
DRAINAGE -80 1 2
INITIAL 1 * 0 0 0
BYPASS 1 1 1
NOISE 0 0.001 INTERNAL
```

Fig. A5.3: simulation script

Execution

The executable of EMERALD should be run in a MS-DOS environment. If your operating system is WINDOWS 3.x/95/98/NT, EMERALD should be executed in a MS-DOS-box. Execution starts after typing

EMERALD <script_file>

on the command-line, followed by pressing the ENTER/RETURN-key. The name of the script file should satisfy the MS-DOS conventions, even when EMERALD is installed on a WINDOWS-machine. File names may contain wildcarts in order to start several script files on a row. For instance

EMERALD *.scr

processes all script files with extension *scr* in the active directory.

Input files

The data flow diagram of EMERALD discerns three (ASCII) input files. The first contains meteorological data, the second observed groundwater levels, and the third soil physical characteristics.

The meteo file consists of four columns, *i.e.* day number (1-365 or 366), year (4 digits), amount of precipitation (mm), and amount of evapotranspiration according to Makkink (mm). An example of a meteo file is given in Figure A5.4. Parameter *skip* equals 1, because one header line is present. Missing values are not allowed. Furthermore, the time step between successive lines should equal 1 day.

day	year	P	ET
1	1959	6.5	0.4
2	1959	9.0	0.3
3	1959	5.4	0.3
4	1959	7.7	0.3
5	1959	7.7	0.3
6	1959	0.5	0.2
7	1959	2.9	0.1
8	1959	12.4	0.3
9	1959	2.7	0.2
10	1959	8.3	0.1

Fig. A5.4: Example of a meteo file

The observation file consists of three columns, *i.e.* day number (1-365 or 366), year (4 digits), and observed groundwater levels (cm). The entries of the third column are defined with respect to the soil surface, and are decreasing in downward direction. All alphanumeric characters (including blanks) are regarded as missing values. An example of an observation file is given in Fig. A5.5. It contains one header line, so parameter *skip* of the OBSERVATION-directive should be set to 1.

day	year	Y
14	1982	-36
28	1982	-34
43	1982	-39
57	1982	-33
74	1982	-39
88	1982	
104	1982	-64
118	1982	-71
134	1982	-74
148	1982	-90

Fig. A5.5: Example of an observation file

The file containing soil physical properties is called "Staring.dat". This file contains the Van Genuchten parameters, the critical depth, and the thickness of the capillary fringe for all soil building blocks of the "Staringreeks" (Wösten *et al.*, 1994). The user is allowed to add new building blocks, and edit existing ones. However, see to it that the codes referring to the soil building blocks consist of three characters at most.

```
STARINGREEKS, Wösten et al., 1994 (Technical Document 18)

topsoils
code      θr       θs       Ks        α         l         n        zc       dae
B1      0.01     0.43    17.46    0.0249    -0.140     1.507     94.0      19.2
B2      0.02     0.43     9.65    0.0227    -0.983     1.548    104.0      18.8
B3      0.01     0.45    17.81    0.0152    -0.213     1.412    151.0      19.3
B4      0.01     0.42    54.80    0.0163     0.177     1.559    201.3      19.8
B7      0.00     0.40    14.07    0.0194    -0.802     1.250     93.2      18.0
B8      0.00     0.43     2.25    0.0096    -2.733     1.284    102.3      15.1
B9      0.00     0.43     1.54    0.0065    -2.161     1.325    119.1      15.0
B10     0.01     0.42     1.17    0.0118    -4.795     1.224     58.2      10.8
B11     0.00     0.60     5.26    0.0243    -5.395     1.111     29.0      10.5
B12     0.00     0.55    15.46    0.0532    -8.823     1.081     24.5      10.2
B14     0.01     0.42     0.80    0.0051     0.000     1.305     65.0      12.3
B16     0.00     0.73    13.44    0.0134     0.534     1.320    120.4      18.8
B17     0.00     0.72     4.46    0.0180    -0.350     1.140     30.0      11.9
B18     0.00     0.77     6.67    0.0197    -1.845     1.154     43.9      14.0

subsoils
code      θr       θs       Ks        α         l         n        zc       dae
O1      0.01     0.36    13.21    0.0224     0.000     2.167     87.0      19.5
O2      0.02     0.38    15.56    0.0214     0.039     2.075     96.0      19.6
O3      0.01     0.34    18.30    0.0211    -0.522     1.564    127.0      19.4
O4      0.00     0.36    53.10    0.0216    -0.520     1.540    189.0      19.8
O5      0.01     0.32    43.55    0.0597     0.343     2.059     42.0      19.4
O6      0.00     0.41     5.48    0.0291    -6.864     1.152     61.6      12.4
O8      0.00     0.47     9.08    0.0136    -0.803     1.342    128.3      18.5
O9      0.00     0.46     2.23    0.0094    -1.382     1.400    107.0      16.3
O10     0.00     0.49     2.22    0.0107    -2.123     1.280     79.1      14.7
O11     0.00     0.42    13.79    0.0191    -1.384     1.152     66.5      16.3
O12     0.00     0.56     1.14    0.0095    -4.171     1.159     33.1       8.9
O13     0.00     0.57     3.32    0.0171    -4.645     1.110     25.1       9.6
O14     0.00     0.38     0.36    0.0025     0.057     1.686    140.0      12.2
O15     0.01     0.41     3.70    0.0071     0.912     1.298    109.2      17.1
O16     0.00     0.89     1.07    0.0103    -1.411     1.376     58.1      13.2
O17     0.00     0.86     2.75    0.0127    -1.832     1.274     71.0      15.0

user defined soils
code      θr       θs       Ks        α         l         n        zc       dae
D1      0.01     0.43    17.46    0.0249    -0.140     1.507     94.0      19.2
W1      0.01     0.36    13.21    0.0224     0.000     2.167     87.0      19.5
```

Fig. A5.6: Example of "Staring.dat"

Output files

EMERALD always generates an ASCII output file. It contains a summary of input data, and the results of executed calibration, prediction and/or simulation routines. In case of simulation, the results can also be stored in binary (direct-access) format by using the BINARY-directive. The contents of each record is given in table A5.1.

Table A5.1: Contents of binary (direct-access) files. Each record contains 4 bytes of information.

record	contents
0	first year of the simulation period
1	final year of the simulation period
2	number of runs
3-eof	realizations, where the year-loop is embedded in the run-loop

Concluding remarks

Although EMERALD has been extensively tested, it is not guaranteed free of bugs. If errors or imperfections are encountered, please inform the authors. The authors and SC-DLO disclaim all liability for direct, incidental, or consequential damages resulting from using EMERALD.